THESIS FOR THE DEGREE OF LICENTIATE OF ENGINEERING IN PHYSICS

Dynamics of High-Angle Grain Boundary YBCO Josephson Junctions

Tobias Lindström

Department of Microtechnology and Nanoscience
CHALMERS UNIVERSITY OF TECHNOLOGY AND GÖTEBORG UNIVERSITY
Göteborg, Sweden 2004

Dynamics of High-Angle Grain Boundary YBCO Josephson Junctions
Tobias Lindström

Technical report no: GIPR-379
Department of Microtechnology and Nanoscience
Chalmers University of Technology and Göteborg University
SE-412 96 Göteborg
Sweden
Telephone +46 (0)31-772 1000

ISSN: 0280-2872

Chalmersbibliotekets reproservice
Göteborg, Sweden 2004

Dynamics of High-Angle Grain Boundary YBCO Josephson Junctions
TOBIAS LINDSTRÖM
Department of Microtechnology and Nanoscience
Chalmers University of Technology and Göteborg University
Göteborg, Sweden 2004

Abstract

This thesis describes experimental investigations of properties of high-angle $YBa_2Cu_3O_{7-\delta}$ (YBCO) bicrystal Josephson junctions and SQUIDs fabricated on $SrTiO_3$-substrates. The main focus of the investigation has been on the effects of the predominant d-wave symmetry of the superconducting wavefunction in YBCO on transport properties and dynamics.

At a high-angle grain-boundary interface between two high-temperature superconductors Andreev states can form, the current carried by these states has π-periodic component which flows in a direction opposite of the usual Josephson current. Asymmetric high-angle grain boundaries also exhibit a critical current which is four orders of magnitude lower than symmetric lower-angle junctions, this can be attributed to the node-lobe arrangement of the the superconducting order parameter.

High-angle grain-boundary dc-SQUIDs that have been studied which exhibit unusual dynamics such as a relative ”shift” of the positions of the positive and negative modulation and a highly non-sinusoidal dependence on the external field. This behavior vanished when moving to very narrow junctions. These result are explained using a semi-classical model which assumes the presence of a 2^{nd} harmonic in the current-phase relation. Numerical simulations confirm that this model is in qualitative agreement with experimental results.

The properties of sub-micron sized junctions have also been studied. These exhibit some unusual behavior. These junctions have been used to study the tunnelling spectra since the high normal resistance means that it is possible to study energies close to the gap.

Finally, some general properties of high-angle Josephson Junctions are discussed. It is argued that some seemingly inconsistent experimental results can be explained using a multi-channel model which accounts for the wiggling and faceting of the interface.

Keywords: Josephson Junctions, High-Temperature Superconductivity, Andreev States, Intrinsic effects, SQUID dynamics

...quantum phenomena do not occur in Hilbert space, they occur in a laboratory.
-Asher Peres

LIST OF APPENDED PAPERS

I. A.Ya. Tzalenchuk, T. Lindström, S.A. Charlebois, E.A. Stepantsov, A.M. Zagoskin, Z. Ivanov and T. Claeson,
”Feasibility studies of ultra-small Josephson junctions for qubits”,
IEEE Transactions on Applied Superconductivity, v 13, n 2 (2003)

II. T. Lindström, S. A. Charlebois, A. Ya. Tzalenchuk, Z. Ivanov, M. Amin and A.M. Zagoskin,
”Dynamical Effect of an Unconventional Current-Phase Relation in YBCO dc SQUIDs”
Physical Review Letters 90, 117002 (2003)

III. A. Ya. Tzalenchuk, T. Lindström, S.A. Charlebois, E.A. Stepantsov, Z. Ivanov and A.M. Zagoskin,
”Mesoscopic Josephson Junctions of high-Tc Superconductors”
Physical Review B 68 100501(R) (2003)

Contents

1 Introduction **11**
- 1.1 High Temperature Superconductivity . . . 11
  - 1.1.1 Conventional Superconductivity . . . 13
  - 1.1.2 Symmetry and Topology of the Wavefunction in YBCO . . . 13
- 1.2 Applications of High Temperature Superconductors . . . 14

2 Theory and Background **16**
- 2.1 The Josephson Effect and Conventional Junctions . . . 16
  - 2.1.1 Derivation of the Josephson Equations . . . 16
  - 2.1.2 The AC Josephson Effect . . . 18
- 2.2 General Properties of the Josephson Current-Phase Relation . . . 19
  - 2.2.1 Types of Junctions and the transparency of the barrier . . . 20
- 2.3 Quantum Interference Devices . . . 21
  - 2.3.1 The dc-SQUID . . . 21
- 2.4 Dynamics of Junctions and SQUIDs . . . 22
  - 2.4.1 The Washboard-potential model . . . 23
- 2.5 The Influence of a 2^{nd}-harmonic . . . 25
  - 2.5.1 Dynamics of dc-SQUIDS in the presence of a 2^{nd} harmonic in the CPR . . . 26
  - 2.5.2 Numerical calculations . . . 27
  - 2.5.3 Junctions in magnetic fields . . . 28
- 2.6 HTS Josephson Junctions . . . 32
  - 2.6.1 Grain Boundary Josephson Junctions . . . 32
  - 2.6.2 J_c vs. angle for grain boundaries: d-wave effects . . . 34
  - 2.6.3 Excess current . . . 35
  - 2.6.4 Andreev states . . . 35
- 2.7 Some further properties of GBJJ . . . 38
- 2.8 Motivation for this work . . . 38

3 Experimental **39**
- 3.1 Device Fabrication . . . 39
  - 3.1.1 Lithography . . . 39
  - 3.1.2 Sample design . . . 40
  - 3.1.3 Considerations . . . 41

3.2 The Measurement setup 41

4 Experimental Results **44**
4.1 Properties of High-Angle Junctions 44
4.1.1 Electrical Transport Properties 45
4.2 High-Angle Grain Boundary SQUIDs 47
4.2.1 High-Field properties 47
4.2.2 Low-field properties 47

5 Discussion **52**
5.0.3 A multi-channel transport model 52
5.0.4 Submicron junctions 53

6 Summary and Outlook **54**
6.1 Future Experiments 54
6.1.1 Implications of this work 55
6.2 A HTS Qubit? 55

7 Acknowledgements **56**

A Energy Conversion Table **61**

B Numerical Calculations **62**

C Appended Papers **65**

Definitions of symbols and how they are used in this thesis

Φ_0	Flux quantum $h/2e$
Φ	Total magnetic flux through a loop
Φ_x	Flux generated by an external field
ϕ_x	Normalized flux $2\pi\Phi/\Phi_0$
θ	Phase of the superconducting wavefunction in a electrode
ϕ	Superconducting phase difference across a junction $\theta_2 - \theta_1$
Ψ	Superconducting wavefunction
I	Bias current
I_c	Critical current of a Josephson junction
I_s	Supercurrent
I_m^n	Our notation for the current components in a SQUID, subscript m=1,2 denotes the junction and superscript n=I, II is the 1^{st} or 2^{nd} harmonic.
α_m	I^{II}/I^I for junction m
η	E_2^I/E_1^I
j_c	Critical current density
R_N	Normal resistance of a Josephson junction
ρ_N	Normal resistivity
T_c	Critical temperature of a superconductor
l	Mean free path of an electron
V	Voltage
U	Free energy
E_J	Josephson energy
E_c	Charging energy of a Josephson junction
λ	Magnetic penetration depth
λ_J	Josephson penetration depth
ω_p	Plasma frequency

Chapter 1

Introduction

The discovery of the high-temperature superconductors (HTS) in 1986 was a major event in the history of solid state physics. Before the famous paper by Bednorz and Müller [1] many had thought that superconductivity at temperatures above approximately 40K was impossible. In 1986 a good theoretical framework existed that could be used to understand almost every aspect of the behavior of convectional, low-temperature, superconductors (LTS) and people immediately set out trying to understand this new class of materials using these well-known theories. However, it was soon realized that even though high-temperatures superconductors share most of their traits with conventional superconductors and at first appeared to behave like type-II superconductors; there were subtle differences that would turn out to be very important. These differences between high- and low-temperature superconductors would hamper the possibility of using HTS in applications but at the same time open up a new field of physics.
Soon after the discovery of HTS the first HTS Josephson Junctions were fabricated (see for example [2]), the first devices were made using point-contact or break-junction techniques but soon thereafter bicrystal junctions were successfully fabricated and characterized. Hence the basis for the bicrystal technique that has been used in this work has been around for more than 15 years but it continues to be a versatile and useful tool.
The predominant d-wave symmetry in YBCO gives rise to a large number of interesting effects. By controlling the orientation of the electrodes, various phenomena can be studied and used. The "high-angle" junctions, where the total misorientation angle is close to 45^o, are especially interesting. In this thesis the properties of high-angle bicrystal YBCO junctions will be discussed. It will be shown that these junctions can behave in a way which is quite different from what is found in both conventional superconductors and lower angle HTS junctions. The possibility of using some of these effects in applications will also be discussed.

1.1 High Temperature Superconductivity

All known HTS are oxides[1] and have a layered structure. The first material to be discovered was La-doped barium cuprate $La_4BaCu_5O_{13}$ (LBCO) which had a transition temperature, T_c, of 35 K. A few months later it was shown that the related material $YBa_2Cu_3O_{7-\delta}$ ("YBCO") had a T_C of 92K. By now many more materials have been discovered including electron- and hole-doped compounds.

[1] There are non-oxide superconductors with structures similar to the HTS, but T_c is usually very low.

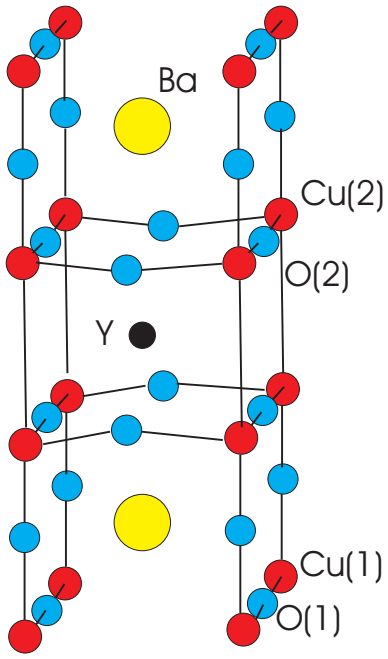

Figure 1.1: The structure of YBCO. The ions labeled with a (1) belong to the chains whereas (2) belong to the superconducting Cu-O planes

YBCO together with the bismuth compound BSCCO are however still the most important materials for applications, even though the highest T_c is found in quicksilver compounds.
Structurally the HTS superconductors belong to a family known as the perovskites. They are layered compounds incorporating Cu-O planes, it is in these planes the superconductivity occurs. The other planes probably serve as ”spacers” between the layers and charge reservoirs for the Cu-O planes.
The structure of materials such as YBCO means that it is often useful to think of HTS as being quasi 2-dimensional. This model is especially useful when describing the properties of epitaxial thins films, most of the physics can be understood by imagining that the film consists of a single plane of Cu-O. Note however that there are many effects that can only be understood by considering the full 3D lattice.

YBCO

YBCO is the most common HTS. It is used both in applications and in basic research. The reason for its popularity is itS relatively high T_c (92K) and it is relatively easy to fabricate high-quality thin films and devices. Over the years many methods for depositing epitaxial YBCO films have been developed. For example Pulsed Laser Deposition (PLD), sputtering, co-evaporation and MBE.
YBCO is a very ”typical” HTS. It is a perovskite with a layered structure as shown in fig. 1.1 which is orthorhombic in the superconducting phase. In the center there is a yttrium ion surrounded by two Cu-O planes. The superconducting transport takes place in these planes. Above/below the planes there are two additional planes with barium-oxide and finally a layer with CuO_x chains.
The stoichiometric phase of YBCO is $YBa_2Cu_3O_6$ which is tetragonal and not superconducting. In order for YBCO to become superconducting it must be doped with additional oxygen which will find sites in the interleaved layers, the resulting compound is $YBa_2Cu_3O_{7-\delta}$ where δ must be below 0.6

in order to form the superconducting orthorhombic phase, if δ is bigger than that the compound is in an antiferromagnetic phase. Optimally doped YBCO has 0.16 holes per copper atom corresponding to 1.15 holes per unit cell. YBCO in the superconducting phase is semi-metallic above T_C, hence it is a rather poor conductor.
The most important lesson from the complicated chemistry of YBCO is that one has to take care to preserve the oxygen content during device fabrication. Even an optimally doped film can loose its oxygen if, for example, it is heated too much (the ”limit” is around 140° C in normal atmosphere). Another problem is that other oxide materials such as STO can ”suck” oxygen from YBCO if deposited on top, this is a serious problem when making multilayer devices. The diffusion length of oxygen in YBCO is rather large even at moderate temperatures which means that it is difficult to preserve the oxygen content in small structures, the linewidth seems to be limited to around 50-100 nm for a 200 nm thick film; structures with a width below that are not superconducting, most likely this is due to oxygen out-diffusion.

1.1.1 Conventional Superconductivity

Conventional superconductivity was discovered by Kamerlingh Onnes in 1911. Onnes was studying the low-temperature properties of mercury and noticed a sudden drop in resistivity when the temperature dropped below 4.15K.
It took a long time for a complete theory to be developed. The first theories were phenomenological and assumed the existence of a ”superfluid” in the superconductor. A microscopic theory of conventional superconductivity [2] was first published in 1957 by Bardeen, Cooper and Schrieffer[3], it is now simply known as the BCS-theory. Using BCS-theory one can explain most properties of a conventional superconductor.
A superconductor differs from normal materials in that it is characterized by a single, macroscopic, wavefunction. The whole superconductor, no matter how large it is, will in the absence of any weak links be in the same quantum mechanical state; the electrons form what is known as a *condensate*.
The mechanism behind conventional superconductivity is that two electrons under the right circumstances can form what is known as a Cooper pair. This happens at at a temperature below a critical temperature T_c where a weak *attractive* force, in conventional superconductors mediated by phonons, can act between electrons near the Fermi level. The orbital state of the Cooper pair can have a radius ξ_0 which is very large, of the order of a micron. The Cooper pair is a boson which means that it is possible for many pairs to condense into the same quantum state.
Soon after the discovery of high-temperature superconductivity in 1986 it became clear that the new class of materials can *not* be explained using the simple BCS-theory. HTS and conventional superconductivity do have many things in common, we know for example that the existence of superconductivity in HTS materials is due to the electrons forming Cooper pairs and creating a condensate, just as in BCS-superconductors. There are however also many differences and at present no one knows how to explain *why* the electrons decide to form a condensate in the first place. This is still one of the most important problems in physics.

1.1.2 Symmetry and Topology of the Wavefunction in YBCO

The existence of a condensate is the reason for the existence of superconductivity. A condensate can always be described by a singe macroscopic wavefunction, also known as the order parameter. The

[2] With ”conventional” we mean low temperature superconductors including MgB_2, another common name is ”BCS-superconductor”.

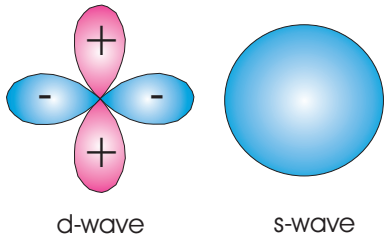

Figure 1.2: Polar diagram of the variation of the gap δ_k. *Left*: d-wave symmetry with four lobes and alternating sign of the order parameter. *Right*: s-wave (singlet) pairing, the gap is isotropic.

simplest way of understanding this concept is to consider it to be a description of the centre of mass motion of the Cooper pair. A more formal description [4] can be given by looking at the expectation value $< \psi^{\dagger}(\mathbf{r'})\psi(\mathbf{r}) >$, this usually falls of very rapidly as **r'** is separated from **r** because the phase factors from different terms tend to cancel, but in a superconductor this is not the case; the pair function in BCS theory has the property that the condensed pair retains an expectation value even for large $|\mathbf{r'} - \mathbf{r}|$ and this is what is meant by long range phase coherence. It can also be shown that the pair function is an effective wavefunction for a large number of particles.
The BCS theory assumes a singlet (s-wave) pair function [3]. However, it is now generally accepted that the wavefunction in HTS such as YBCO does not have this simple shape, evidence from many experiments has shown that the wavefunction is not just strongly anisotropic, but also topologically complicated.
The symmetry of the crystal lattice in for example YBCO limits the number of possible symmetries of the wavefunction to s,p and d (here we are using the same notation as is used to label the electronic orbitals in atomic physics). Using Knight-shift measurement the possibility of a a p-symmetry was eliminated, hence the wavefunction could only have s- or d-wave symmetry.
Using phase sensitive techniques such as π-SQUIDs, corner junctions [5] and tricrystal rings[6] it was possible to establish that the phase changes sign as one moves around the Fermi surface and that the gap-function vanishes in the four $< 110 >$ directions, furthermore there is a phase change of π for rotation around the *z*-axis.
Based on symmetry-considerations and experimental data various forms of the wavefunction have been suggested: Anisotropic s, extended s, d_{xy}, $d_{x^2-y^2}$ and admixtures such as $d + s$ and $d + is$ (i.e. an imaginary s-component), but today most people agree that the $d_{x^2-y^2}$-symmetry is the correct form; possibly with an admixture of a very small s-component (which should exist in an orthorhombic crystal[7]). An illustration of a $d_{x^2-y^2}$ wavefunction can be seen in figure 1.2. There are four lobes with alternating sign and four nodes where the gap disappears.

1.2 Applications of High Temperature Superconductors

Superconductivity was discovered almost 100 years ago and even though it has been an active area of research ever since, few applications have actually left the laboratory, a notable exception is superconducting magnets used in for example MRI which today can be found in all major hospitals. The problem is of course that you need to cool the superconductor to very low temperatures, conventional superconductors are usually operated at 4.2K. The advent of high temperature

[3]The BCS-theory itself is a very general and pair functions of any symmetry can be used, but when describing conventional superconductors a singlet wave-function is used

superconductivity promised to change this and bring superconductivity to the general public, now it would be enough to cool the devices using inexpensive liquid nitrogen. Unfortunately, it turned out to be more difficult than that and HTS superconducting devices are still rare 17 years after the discovery. However, superconductivity is slowly making its way into the real world[8]. There are for example important medical applications where HTS devices, predominantly SQUIDs , are starting to be used. Magneto Cardiography (MCG) and Magneto encephalography (MEG) are used to study the heart and brain respectively. Other examples include superconducting filters which are being tested for use in base stations for mobile phones. So far the most promising market for HTS is probably power applications such as power transmission cables, transformers and engines.
In order to fulfill the promises of high temperature superconductivity more research is still needed. We still do not understand the mechanism behind HTS and there are other fundamental issues that need to be resolved, hopefully solving these problems will make it possible for more applications to reach a stage where they can be used in the everyday world.

Chapter 2

Theory and Background

In 1962 [9] Brian Josephson predicted two new effects that can occur when two superconductors are connected through a insulator. In his calculations he showed that a zero voltage supercurrent can flow through the barrier, he also predicted that if the junction is biased with a voltage V a phase difference would evolve in time. These predictions are now known as the dc- and ac Josephson effects. It did not take long before the theory was experimentally verified and the field grew rapidly. Today it is a rich and well-developed field of physics.
It was soon realized that the Josephson effect can occur in a wide variety of situations, it is enough to have two superconductors connected through a *weak link*, a region where the superconductivity has been suppressed somehow. Since the effect can occur in such a wide variety of situations the general theory is rather complicated (especially since the mechanisms which carry the supercurrent differ between different types of barriers) and usually the calculations are simplified by assuming that one is working in a certain mathematical limit. Hence, what will be discussed here are only some special cases of a much more general theory.

2.1 The Josephson Effect and Conventional Junctions

The situation analyzed by Josephson is illustrated in figure 2.1. Two superconducting electrodes are separated by a very thin insulating barrier. If the barrier is thick no current can flow; but if the layer is thin enough there will be an appreciable quantum mechanical amplitude for the electrons to ”crawl under” (tunnel) the barrier.
In terms of wavefunctions one can think of the situation as follows: In each of the electrodes we have a superconducting wavefunction which will extend somewhat into the barrier (this is just another example of a quantum mechanical penetration of a barrier) , therefore in a thin barrier we can have a situation where the tails of the wavefunctions will overlap which in turn means that they can interact. As we will see the end result is that we can have a supercurrent flowing through a barrier.

2.1.1 Derivation of the Josephson Equations

In his famous *Lectures*[10] Feynman derived the Josephson equations in a very clear and concise manner. The derivation used here follows that of Feynman very closely but has been slightly modified in anticipation of the discussion in section 2.2.

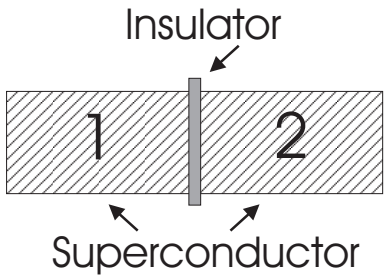

Figure 2.1: Two superconductors separated by a thin insulator, the simplest form of a Josephson Junction.

Suppose we have two identical superconductors separated by an thin insulator as depicted in figure (2.1). Assuming there is no applied magnetic field and everything is symmetric [1] we can argue that the superconducting wavefunctions on each side of the junction should be weakly coupled with a strength K. Hence, we can write two coupled equations for the amplitudes on each side of the insulator

$$i\hbar\frac{\partial\Psi_1}{\partial t} = U_1\Psi_1 + K\Psi_2 \tag{2.1a}$$

$$i\hbar\frac{\partial\Psi_2}{\partial t} = U_2\Psi_2 + K\Psi_1 \tag{2.1b}$$

In equilibrium the energy U_1 is of course equal to U_2 and nothing happens. If we bias the junction with a voltage V the energies will be shifted so that $U_1 - U_2 = qV$ where q is the charge of the current carrying particle. For convenience we can define zero of energy to be halfway between between U_1 and U_2

$$i\hbar\frac{\partial\Psi_1}{\partial t} = \frac{qV}{2}\Psi_1 + K\Psi_2 \tag{2.2a}$$

$$i\hbar\frac{\partial\Psi_2}{\partial t} = -\frac{qV}{2}\Psi_2 + K\Psi_1 \tag{2.2b}$$

In order to solve this system of equations we make to following *ansatz*

$$\Psi_l = \sqrt{\rho_l}e^{il\theta} \tag{2.3a}$$

$$\Psi_m = \sqrt{\rho_m}e^{im\theta} \quad l, m \in \mathbf{Z}$$

By inserting these expressions into (2.3) we get

$$\sqrt{\rho_n}e^{il\theta_1}\left(\frac{i\hbar\dot{\rho}_l}{2\rho_l} - l\hbar\dot{\theta}_1 - \frac{qV}{2}\right) = K\sqrt{\rho_m}e^{im\theta_2} \tag{2.4a}$$

$$\sqrt{\rho_m}e^{im\theta_2}\left(\frac{i\hbar\dot{\rho}_m}{2\rho_m} - m\hbar\dot{\theta}_2 + \frac{qV}{2}\right) = K\sqrt{\rho_n}e^{im\theta_1} \tag{2.4b}$$

By equating the real and imaginary parts we get four equations

$$\dot{\rho}_l = \frac{2K}{\hbar}\sqrt{\rho_m\rho_l}\sin(m\theta_2 - l\theta_1) \tag{2.5a}$$

$$\dot{\rho}_m = -\frac{2K}{\hbar}\sqrt{\rho_m\rho_l}\sin(m\theta_2 - l\theta_1) \tag{2.5b}$$

$$l\dot{\theta}_1 = \frac{K}{\hbar}\sqrt{\frac{\rho_m}{\rho_l}}\cos(m\theta_2 - n\theta_1) - \frac{qV}{2\hbar} \tag{2.5c}$$

$$m\dot{\theta}_2 = \frac{K}{\hbar}\sqrt{\frac{\rho_l}{\rho_m}}\cos(m\theta_2 - l\theta_1) + \frac{qV}{2\hbar} \tag{2.5d}$$

[1] Another, implicit, assumption is that time-reversal symmetry is preserved.

The current through the junction must be equal to the change in density and is therefore equal to $\dot{\rho_l} = -\dot{\rho_m}$. Letting $n\phi = m\theta_2 - l\theta_1$ ($n \in \mathbf{Z}$) we can write this as

$$\frac{2K}{\hbar}\sqrt{\rho_m \rho_l}\sin n\phi = J_n \sin n\phi \tag{2.6}$$

where we have introduced the constant J_n to represent the density of supercurrent flowing through the junction. Now, we have in fact solved the system for an *arbitrary* $n \in \mathbf{Z}$ and have therefore obtained a set of solutions, since the system is linear that means that the most general solution is given by the sum of these solutions

$$J = \sum_{n=1}^{\infty} J_n \sin n\phi \tag{2.7}$$

By calculating the difference $m\dot{\theta}_2 - l\dot{\theta}_1 = n\dot{\varphi}$ we obtain another interesting equation

$$\frac{d\phi}{dt} = \frac{2e}{n\hbar}V \tag{2.8}$$

Where we have used the fact that $q = 2e$ in a superconductor (the charge-carrying "particle" is the Cooper pair). Eq. 2.7 and 2.8 are the celebrated **Josephson equations**, and are known as the dc- and ac Josephson effect respectively. Here we have written the equations in their most general form, usually it is assumed that only the first harmonic gives a contribution to the total current giving

$$I = I_c \sin\phi \tag{2.9}$$

$$\frac{d\phi}{dt} = \frac{2e}{\hbar}V \tag{2.10}$$

where we have written an expression for the total current in the junction and introduced I_c, the *critical current* of the junction. This is the most common form of these equations.
Equation 2.7 is the most general way of writing what is known as the *Current-Phase Relation* (CPR) of a junction. The CPR simply tells us how the current through the junction changes with phase, it is an important concept and the focus of this work.

2.1.2 The AC Josephson Effect

The notion of an "AC Josephson Effect" is actually a bit misleading. The DC- and the AC effects are in reality just consequences of the same physical mechanism. The name refers to the fact that when the amount of current passing through the junction exceeds I_c the junction will switch from the supercurrent state (or "S-state") to a resistive state ("R-State"). Hence, a voltage will appear over the junction. We can see from Eq. (2.6) and (2.8) that the voltage will oscillate in time. Using eq. (2.8) one can easily show that the oscillation frequency will be given by $2e/n\hbar$ multiplied by the voltage, this number is equal to 483.61 GHz/mV which means that the junction is emitting radiation at frequencies close to the far-infrared part of the spectrum. A Josephson junction essentially behaves as a voltage controlled oscillator; the only parameters appearing in the expression for the frequency are natural constants. It is only when we look at the *average* voltage over the junction that we will see a dc-voltage, since the oscillation frequency is so high you need dedicated microwave detectors in order to measure the microwave radiation coming from the junction.
An important consequence of the AC Josephson effect is that when we irradiate the junction with microwaves the external radiation will mix with the internal oscillations causing what is known as Shapiro steps to appear on the IV-curve at, the steps will appear at all voltages $V = mh/2ef_{ext}$ [11],

however the amplitude of these steps decreases as m increases so usually only the first few steps are visible.
It is important to remember that a Josephson junction is intrinsically a microwave-device even when we are only interested in the dc-properties. LC-resonances, Fiske-steps [12] and other microwave-induced phenomena are frequently seen in dc current-voltage characteristics. Another, quite subtle, problem is that when considering how the properties of for example the substrate is affecting a device one sometimes has to use the high-frequency permittivity of the material which can differ considerably from the dc-value.

2.2 General Properties of the Josephson Current-Phase Relation

Regardless of the material, geometry or transport mechanism giving rise to the Josephson effect in a junction there are several general properties that must be true for all theoretical models used to describe the process.

- Changing the phase across the junction by 2π should not change the physical state of the junction. Hence, the change must not influence the supercurrent across the junction and the CPR is a 2π-periodic function
$$I_S(\phi) = I_S(\phi + 2\pi) \tag{2.11}$$

- Changing the direction of flow of the supercurrent must change the sign of the phase, whence
$$I_S(\phi) = -I_S(-\phi) \tag{2.12}$$
Equation 2.12 does not hold in junctions where the time-reversal symmetry is broken(TRSB) . There are potentiality several mechanisms that can cause this symmetry to be broken in HTS junction, it was for example shown that the presence of an imaginary subdominant components of the order parameter [13] would cause TRSB. More recently Löfwander *et al.*[14] and Amin [15] *et al.* showed that spontaneous TRSB can also occur in pure d-wave junctions. However, so far there is no clear experimental evidence of TRSB in HTS junctions, more experimental data is needed to resolve this issue. In the following discussion it is assumed that eq. 2.12 holds.

- A dc supercurrent can only flow if there is a change of the phase of the order parameter as one crosses the barrier, this means that if $\phi = 0$ there should be zero supercurrent
$$I_S(2\pi n) = 0,\ n = 0, \pm 1, \pm 2... \tag{2.13}$$

To summarize the supercurrent in the absence of TRSB must be a symmetric 2π-periodic function, therefore it can always be expanded in a Fourier series

$$I_S(\phi) = \sum_{n \geq 1} I_n \sin(n\phi) \tag{2.14}$$

This equation is identical to eq. (2.6), the difference being that now we have derived the result based on *general* principles, hence equation (2.6) is actually valid under quite general assumptions.

Type	Name	Comment
Superconductor-Insulator-Superconductor	SIS	A.k.a. a superconducting tunnel junction
Superconductor-Normal Metal-Superconductor	SNS	
Superconductor-"weak Superconductor"-Superconductor	SS'S	The barrier is e.g. made of a material with lower T_c
Superconductor-Ferromagnet-Superconductor	SFS	Used to study pair-breaking and to make so-called π-junctions
Superconductor-Constriction-Superconductor	ScS	A constriction is a very narrow, -quasi 1D- current channel

Table 2.1: The most common typers of conventional Josephson Junctions

2.2.1 Types of Junctions and the transparency of the barrier

There are many types of Josephson Junctions, some are mere curiosities but a few types are frequently used in applications. The various types of junctions can divided into a few categories depending on the type of electrodes and barriers used. The most common types as well as an explanation of the nomenclature can be found in table 2.1.

The situation is not always as clear-cut however, there is a gradual change between SIS and SNS junctions; both types can be described using BTK-theory [16] (after Blonder-Tinkham-Klapwijk). In BTK-theory the barrier is characterized by a parameter T known as the transparency. If T=0 the junction is SIS-type (tunnel regime) and if T=1 it is SNS (ballistic regime). In reality all junctions have T-values somewhere in between and are neither SNS (which would require a perfectly clean interface) or SIS (a perfect insulator).

Estimating the transparency

In order to be able to compare experiment with theory it is important to be able to determine the type of barrier from experimental data. Unfortunately that is sometimes difficult, even estimating the numerical parameter T can be exceedingly difficult when working with HTS junctions.

In the case of HTS junctions one can estimate the transmissivity of the junction from the normal resistance[17].

$$T \approx \frac{\rho_{ab} l}{R_N A} \tag{2.15}$$

where ρ_{ab} is the resistivity in the a-b plane, l is the mean free path, A is the total area of the junction and R_N the normal resistance of the junction. The BTK-model of Josephson junctions is very useful and equations such as 2.15 are frequently used to estimate T in order to compare experimental data with theoretical predictions. Moreover, T (or other parameters with similar meaning) is frequently introduced even in very sophisticated models of junctions. However, one needs to be very careful when describing HTS junctions with a single parameter. It is frequently the case that two ways of estimating T can be orders of magnitude off even when studying a single structure; the reason for this discrepancy is probably the complicated nature of HTS grain boundaries.

2.3 Quantum Interference Devices

One of the unique properties of superconductivity is that it can be described by a *single* wavefunction, even if the superconducting device is macroscopic, coherence is preserved. This has many important implications, one being that if we connect two Josephson junctions to each other using superconducting leads not only will the *amplitude* of the wavefunctions describing each junction be important but also the *phase*. The situation is analogous to two waterwaves colliding; it is not enough to simply sum the amplitudes to get the shape of the resulting wave, one also has to consider their relative phase. Hence the two junctions interact causing what is known as *quantum interference*.

2.3.1 The dc-SQUID

The most common quantum interference device is the dc-SQUID which is short for **S**uperconducting **QU**antum **I**nterference **D**evice[2]. It consists of two junctions in a superconducting loop, see fig. 2.2.

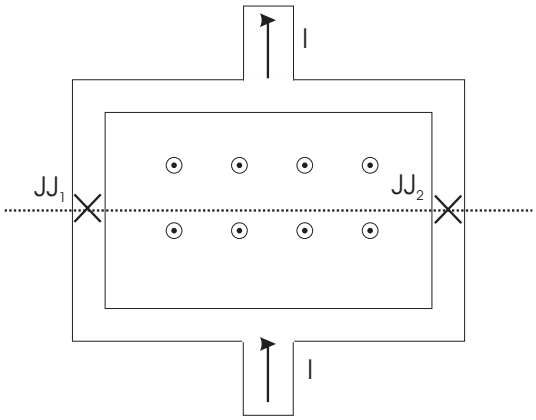

Figure 2.2: A dc-SQUID is created by connecting two Josephson Junctions in a loop. The dotted line would represents the position of the grain boundary if the SQUID was realized using HTS bicrystal junctions.

Inside a bulk superconductor without any holes it can be shown [18] using continuity arguments that the total change of the phase along any closed path is

$$\delta\theta = \frac{2e}{\hbar} \oint \mathbf{A} d\mathbf{l} \equiv 0 \tag{2.16}$$

giving rise to the Meissner effect of ideal diamagnetism of superconductors. Making use of the Stokes theorem

$$\delta\theta = \frac{2e}{\hbar} \oint \mathbf{A} d\mathbf{l} = \frac{2e}{\hbar} \int_S \nabla \times \mathbf{A} dS \tag{2.17}$$

and substituting for $\nabla \times \mathbf{A} \equiv \mathbf{B}$ by definition

$$\delta\theta = \frac{2e}{\hbar} \int_S \mathbf{B} dS = \frac{2e}{\hbar} \Phi = 2\pi \frac{\Phi}{\Phi_0} \equiv 0 \tag{2.18}$$

[2]The other type is known as the *rf-SQUID*, which only incorporates one junction in the loop

In a multiply connected superconductor the continuity argument does not hold, but the wave function must still be single-valued. Hence,

$$\delta\theta = 2\pi\frac{\Phi}{\Phi_0} = 2\pi n \tag{2.19}$$

and the internal flux only takes quantized values in multiples of $\Phi_0 = 2 * 10^{-15}$ Wb.
In a dc-SQUID the phase is not continuous, each junction contributing a certain 'jump' which add up to some value ϕ along the closed path.

$$\delta\theta = 2\pi\frac{\Phi}{\Phi_0} + \phi = 2\pi n \tag{2.20}$$

or ignoring multiples of 2π, which lead to physically equivalent conditions,

$$\phi = -2\pi\frac{\Phi}{\Phi_0} \tag{2.21}$$

and the total phase difference across the junctions, ϕ, (summed with the correct signs along the closed path) becomes flux-dependent. As we know from the previous discussion of the Josephson effect, ϕ is intimately related to the critical current, I_c, which is an experimentally measurable quantity. This and the smallness of Φ_0 makes the SQUIDs extremely sensitive sensors of the magnetic flux. What is more important for this work, the phase difference across the junctions ϕ of a small [3] SQUID is simply proportional to the magnetic flux Φ.

2.4 Dynamics of Junctions and SQUIDs

A very common way of modelling Josephson junctions is to use the so-called resistevly shunted junction (RSJ) model, where the junction is described as being composed of a voltage controlled current source (VCC) in parallel with a resistor, by also adding a parallel capacitor the result is the RCSJ-model which can account for a wide variety of phenomena in Josephson junction. The RCSJ-circuit is composed of the following lumped elements (see figure 2.3).

- A VCC which is governed by the Josephson relations $I = I_s(\varphi)$ and $\dot{\varphi} = 2eV/\hbar$
- A resistor with the value R_N, the normal resistance of the junction.
- A capacitor with a value C, this includes not only the geometrical capacitance but also includes effects of the barrier.

The RCSJ-model is especially useful for the study of dynamics of junctions and SQUIDs, since it is a circuit model it is easy to incorporate for example external inductances.

[3] In this discussion and below we neglect the screening currents in the SQUID loop, i.e., assume that the ratio $\beta = \frac{LI_c}{\Phi_0}$ is small. As the inductance L is mainly determined by the geometry, this means that we are considering small SQUIDs with low critical currents. The internal flux Φ in such small SQUIDs is equal to the externally applied flux Φ_x. Experimentally, in all measured devices β was indeed smaller than 1.

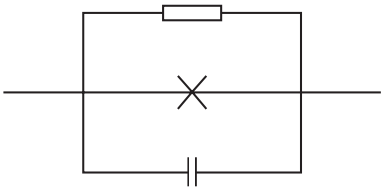

Figure 2.3: The RCSJ-model consists of three lumped elements: R_N, C and a voltage controlled current source. In the simpler RSJ-model the capacitor has been removed.

2.4.1 The Washboard-potential model

Using the RCSJ-model we can write a system of two equations that describe the dynamics of a current biased shunted junction

$$\frac{d\phi}{dt} = \frac{2e}{\hbar}V \tag{2.22a}$$

$$I = I_s(\phi) + \frac{V}{R_N} + C\frac{dV}{dt} \tag{2.22b}$$

This can also be written as a 2nd order equation for the phase

$$\frac{\hbar C}{2e}\frac{d^2\phi}{dt^2} + \frac{\hbar}{2eR}\frac{d\phi}{dt} = I - I_S(\phi) \tag{2.23}$$

In the simplest case the CPR will have the form $I_S(\phi) = I_{C0}\sin\phi$, in this case we can introduce the Stewart-McCumber number

$$\beta_C = \frac{2e}{\hbar}R^2 C I_{C0} \tag{2.24}$$

β_C is important because it determines whether or not the junction is hysteretic. $\beta_C \ll 1$ means that the junction is overdamped and not hysteretic, $\beta_C \gg 1$ means that the junction is heavily underdamped and hysteretic. HTS junctions usually have $\beta_C \approx 1$, i.e. they are slightly hysteretic. The name ”washboard-potential” refers to the fact that the differential equation is similar to the equation for a ball rolling down a tilted washboard, the ”ball” can then be identified with an imaginary ”phase particle”.
If the junction is overdamped we can drop the second order term from the equations. By integrating the result we get the time averaged voltage to be

$$V = R\sqrt{I^2 - I_c^2} \tag{2.25}$$

This is an important equation even though it is simple. It is a fairly good approximation of the behavior of a real junction, the term ”RSJ-like” refers to a junction which exhibits a behavior which can be well described by 2.25. Figure 2.4 shows an example of a slightly underdamped junction. The tilted washboard potential analogy can be carried over to SQUIDs as well [19]. In this case the two junctions are biased to the same voltage, or analogously, the same average washboard slope. The relative phases can be represented by displacement of the two washboards, and this corresponds to the applied flux. The junctions are of course not independent. The relative phase changes adjust themselves to minimize the total energy. This can be modelled by joining the ’phase particles’ by a spring; its stiffness representing the SQUID inductance. In the case of small SQUIDs of negligible

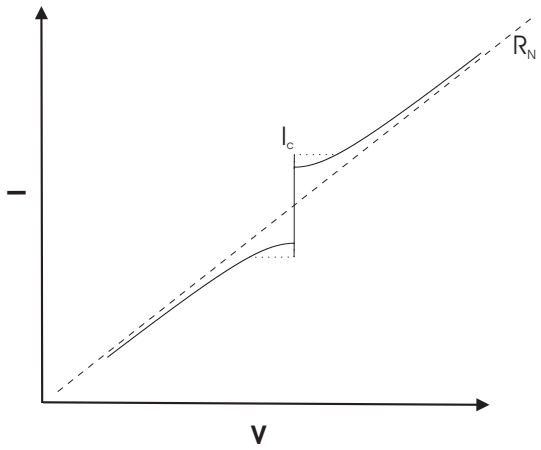

Figure 2.4: An example of an hysteretic (underdamped) IV-curve. The dashed line indicated R_N,the slope of the resistive branch. The switching from the superconducting to the resistive branch has been indicated by a dotted line.

inductance the spring has to be infinitely stiff. This means that the phase *across* the SQUID does not depend on the magnetic field or, equivalently, the phases of the two junctions are 'slaved' to each other. In this respect the small SQUID can be regarded as a single junction with a magnetically adjustable critical current.
It is straightforward to deduce the governing equations for a dc SQUID in the same way . If we assume that both junctions have the same critical current I_c it follows from 2.21 that the maximum critical current through the SQUID will be

$$I_c = 2I_c \left| \cos \pi \frac{\Phi}{\Phi_0} \right| \tag{2.26}$$

If we bias the SQUID above the critical current a voltage will develop across it just as in the case of a single junction. Assuming the junctions are overdamped we can use 2.25 and write

$$V = \frac{R}{2} \sqrt{I^2 - 4I_c^2 \cos^2 \pi \frac{\Phi}{\Phi_0}} \tag{2.27}$$

The washboard potential gets its name from the shape of the energy potential which is shown in figure 2.5. The free energy of a junction can be written

$$E(\phi) = -E_J \cos \phi - \frac{\hbar I}{2e} \phi \tag{2.28}$$

where we have introduced E_J, the Josephson energy which is defined as

$$E_J = \frac{\hbar}{2e} I_c \tag{2.29}$$

The Josephson energy is important because it sets the energy-scale of the behavior, it will also determine how much the dynamics is affected by temperature and noise (a table with energy conversion factors can be found in appendix A). Note that the term $\frac{\hbar I}{2e}\phi$ which corresponds to the "inertia" will disappear if the capacitance is very small, it will therefore be absent in the RSJ-model.

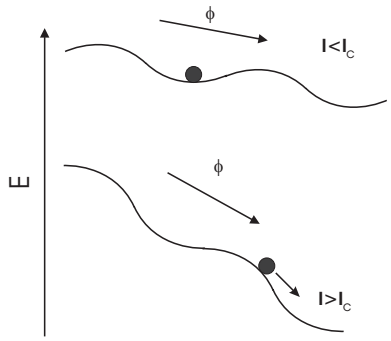

Figure 2.5: The washboard potential model

Using the washboard-potential model we can understand how a junction switches to the resistive state. When $I < I_c$ the ”phase particle” will be trapped in one of the energy minima, but if the ”tilt” of the washboard is gradually increased (by pushing more current trough the junction) we will eventually reach a point where the particle is no longer trapped but will travel along the profile of the potential (known as the ”running state”). The particle can also acquire energy from thermal- or noise-induced fluctuations and this can lead to it going into the running state ”prematurely”, hence in real situations the effective critical current I_c is always lower than the nominal value which is denoted by I_{c0}.

2.5 The Influence of a 2^{nd}-harmonic

Many of the things discussed so far are still valid if we retain higher order terms in (2.14). By including a 2^{nd} harmonic in the CPR we will however change few things.

The possibility of a strong 2^{nd}harmonic (or, equivalently, a π-periodic CPR) in d-wave junctions has been considered in for example [20] [21] [22].

From an experimental point of view the presence of a 2^{nd} harmonic might be difficult to detect when working with single junctions. This is because the junction will always strive to minimize its free energy with respect to the phase and will do so regardless of the exact shape of the current-phase relation. It is therefore difficult to directly see any effect on the dc-properties of a junction. Some parameters ,such as the critical current of the junction, are affected but in most cases these effects are quite small. A junction can, for example, switch to the running state earlier than it would have with a purely sinusoidal CPR, causing a reduction of the measured I_c but that can also happen due to many other reasons.

In order to be able to detect a 2^{nd} harmonic with confidence one has to study the dynamics of the device. In the case of a single junction the most common way is to study the microwave response. This can be an accurate way to detect the presence of a 2^{nd} harmonic since it will cause the appearance of subharmonic Shapiro steps at frequencies $e/\hbar$. This technique has for example been used in [23].

The most sensitive way of studying the effects of the 2^{nd} harmonics is to use quantum interference, this is the technique employed in the work by Il’ichev et al where a RF-SQUID was used [24]. Here we will instead focus on the effects on dc-SQUIDs.

2.5.1 Dynamics of dc-SQUIDS in the presence of a 2^{nd} harmonic in the CPR

When there is a significant contribution from a 2^{nd} harmonic , the equation for the CPR of a dc-SQUID in the presence of an external magnetic field $\phi_x = 2\pi\Phi_x/\Phi$ can be written

$$I_s(\phi, \phi_x) \quad = \quad I_{c1}^I \sin\phi \; - \; I_{c1}^{II} \sin(2\phi) \; + \; I_{c2}^I \sin(\phi \; + \; \phi_x) \; - \; I_{c2}^{II} \sin 2(\phi \; + \; \phi_x) \quad (2.30)$$

Another common way of characterizing SQUIDs is to measure the voltage modulation as a function of applied field. If we limit ourselves to the RSJ-model and introduce the necessary generalizations we can write the average voltage over the SQUID as

$$\bar{V}^{-1} \quad = \quad \frac{G_1 + G_2}{2\pi} \int_{-\pi}^{\pi} d\phi \left[I - (G_1 - G_2)\frac{\hbar}{2e}\frac{d\delta}{dt} \; - I_1\left(\phi + \frac{\delta}{2}\right) - I_2\left(\phi - \frac{\delta}{2}\right)\right]^{-1} \quad (2.31)$$

Here $G_{1,2}$ are the normal conductances of the junctions, and

$$\delta + \phi_x + \frac{\pi L}{\Phi_0}(I_2(\phi - \delta/2) - I_1(\phi + \delta/2)) = 0, \quad (2.32)$$

gives the difference, δ, in phase drops across each junction.

Calculation of the Free energy It is instructive to plot the free energy of this system. In the case of a single junction in the overdamped limit the calculation is straightforward, the relation between the current, energy and phase difference, $I_c(\phi) = (2e/\hbar)\partial E_J/\partial\phi$ follows from gauge invariance (and the Cooper pair charge being 2e) and does not depend on the exact form of E_J. Therefore the Josephson energy of the *n*th harmonic must be equal to $\hbar I_n \cos(n\phi)/(2en)$. Hence, we need to calculate

$$U = \frac{\hbar}{2e}\int_0^{\phi} I(\theta)d\theta \quad (2.33)$$

and, keeping only the first two harmonics

$$E_J(\phi) = -E_J^I\left[\cos(\phi) - \frac{\alpha}{2}\cos(2\phi)\right] \quad (2.34)$$

where the energy scale is set by E_{1J}. As expected the potential will take on the shape of a double well as $\alpha = I_2/I_1$ increases above 1/2.
In the slightly more complicated case of a dc SQUID the phase differences across the junctions will be related to the external flux. Neglecting the self-inductance of the loop the Gibbs free energy of a current-biased dc SQUIDS can then be written [25] [4] as a function of the external phase $\phi_x = \phi_1 + \phi_2$ and a new variable $\gamma = (\phi_1 - \phi_2)/2$ which corresponds to the total phase difference across the SQUID.

$$U(\gamma, \phi_x) = -\varepsilon_\phi\left[\cos\gamma - \frac{\tilde{\alpha_\phi}}{4}\cos(2\gamma)\right] + \tilde{U}(\gamma, \phi_x) \quad (2.35)$$

where

$$\varepsilon_\phi = (1+\eta)\cos(\phi/2) \quad (2.36a)$$

$$\tilde{\alpha_\phi} = [2(\alpha_1 + \eta\alpha_2)\cos\phi]/[(1+\eta)\cos(\phi/2)] \quad (2.36b)$$

$$\eta = E_2^I/E_1^I \quad (2.36c)$$

$$\tilde{U} = -\left[\eta - 1 + 2(\alpha_1 - \eta\alpha_2)\cos\tfrac{\phi}{2}\cos\gamma\right]\sin\tfrac{\phi}{2}\sin\gamma \quad (2.36d)$$

[4] Note that the definition of α differs from that in [25].

Just as in the case of the individual Josephson junctions, the total potential shows a double well behavior as can be seen in figure 2.6.. We still have something which reminds us of a ”tilted washboard” but now there are extra features. If α is small the dynamics will look similar to that of an ordinary junction in the running state, however if α is large enough the ”phase particle” can get trapped *twice* as the phase changes by 2π, this will naturally affect the dynamics of the SQUID.

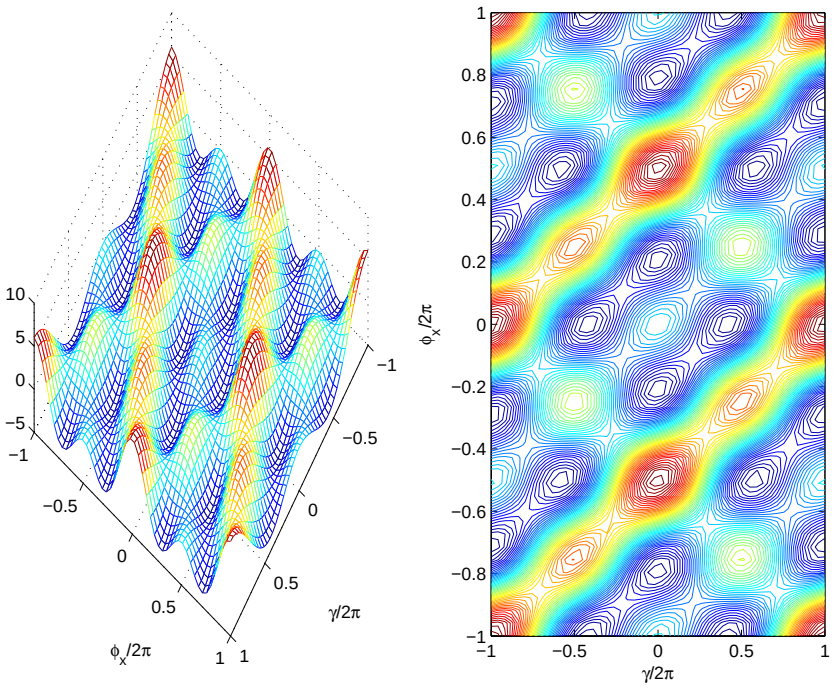

Figure 2.6: Free Energy of a dc-SQUID with $\alpha_1 = \alpha_2 = 2$ and $\eta = 2$. *Left:*3D-plot and *Right:*Contour Plot.

2.5.2 Numerical calculations

Here I will present the results of some numerical simulations that will be used to interpret experimental result later.
We can use eq. 2.30 to calculate the dynamics of a dc-SQUID in the presence of an external field. The critical current is equal to the maximum supercurrent the SQUID can carry

$$I_c(\phi_x) = \max_{\phi} I_s(\phi, \phi_x). \tag{2.37}$$

By using equation 2.37 it is straightforward to numerically calculate the I_c vs. ϕ_x dependence of the SQUID, figure 2.7 shows the results for one of these calculations for a few values of the critical currents. The parameters used can be found in table 2.2.
One can make a few striking observations from these calculations

I. The modulation becomes quasi-π-periodic when the 2^{nd} harmonic is introduced (the true period being 2π unless the first harmonic is exactly zero).

II. The positive and negative curves become shifted with respect to each other, however inversion is still conserved. The maximum I_c is no longer at zero field.

Figure	I_{c1}^{I}	I_{c1}^{II}	I_{c2}^{I}	I_{c2}^{II}
I	1.0	0	1.0	0
II	1.0	0	0	1.0
III	1.0	1.0	1.0	0
IV	1.0	0.5	1.0	0
V	1.0	0.5	0.5	0.5
VI	1.0	0.1	0.2	0.4

Table 2.2: Parameters used to plot figures 2.7 and 2.8.

III. The modulation depth becomes very small when the SQUID is highly asymmetric with respect to junction parameters.

Voltage Response Expression 2.31 can easily be integrated numerically to yield a family of curves which show the modulation for a few values of the bias current, the result can be seen in figure 2.8. Again, one can make a few interesting observations

I. The positive and negative curves are again shifted, inversion symmetry is conserved.

II. The curves become less distorted at high values of the bias, the effects of the 2^{nd} harmonic is "washed out".

III. The modulation depth is again very small.

From these simulations it should be clear that the presence of a 2^{nd} harmonic can affect the dynamics of dc SQUIDS quite dramatically. Note however that the effects are most striking in asymmetric SQUIDs, in the limit of symmetric SQUID where all current is carried by a 2^{nd} harmonic the only effect on the dynamics is that the periodicity doubles, this can be difficult to detect experimentally unless the exact field threading the SQUID-loop is known and it is possible to accurately calculate the expected period of the SQUID (including any flux-focusing effects).

2.5.3 Junctions in magnetic fields

One of the defining facts of a superconductor is that it screens magnetic fields; an applied field will only penetrate a very short distance, known as the *London penetration depth* λ, into the superconductor before it decays completely. The size of λ varies between different superconductors but is about 130 nm for YBCO.
If a Josephson junction is placed in a magnetic field its dynamics will be altered because the field will penetrate a distance λ_J into the junction. λ_J is a screening parameter just as λ and is given by

$$\lambda_J = \sqrt{\frac{\Phi_0}{2\pi J_c \mu_0 (2\lambda + d)}} \tag{2.38}$$

where d is the thickness of the insulating barrier and J_c is the critical current density [5]. $\lambda_J \gg \lambda$ since the Josephson currents are so much weaker than the ordinary superconducting screening currents.

[5] In coplanar junction geometry, such as GBJJ, this expression requires some corrections. It was shown [26] that the expression $\lambda_J = \sqrt{\frac{\Phi_0}{2\pi J_c \mu_0 (2(\lambda^2)/w + d)}}$ (w-width) better describes the experimental data. This expression differs from 2.38 by a factor $\sqrt{w/\lambda} \gg 1$.

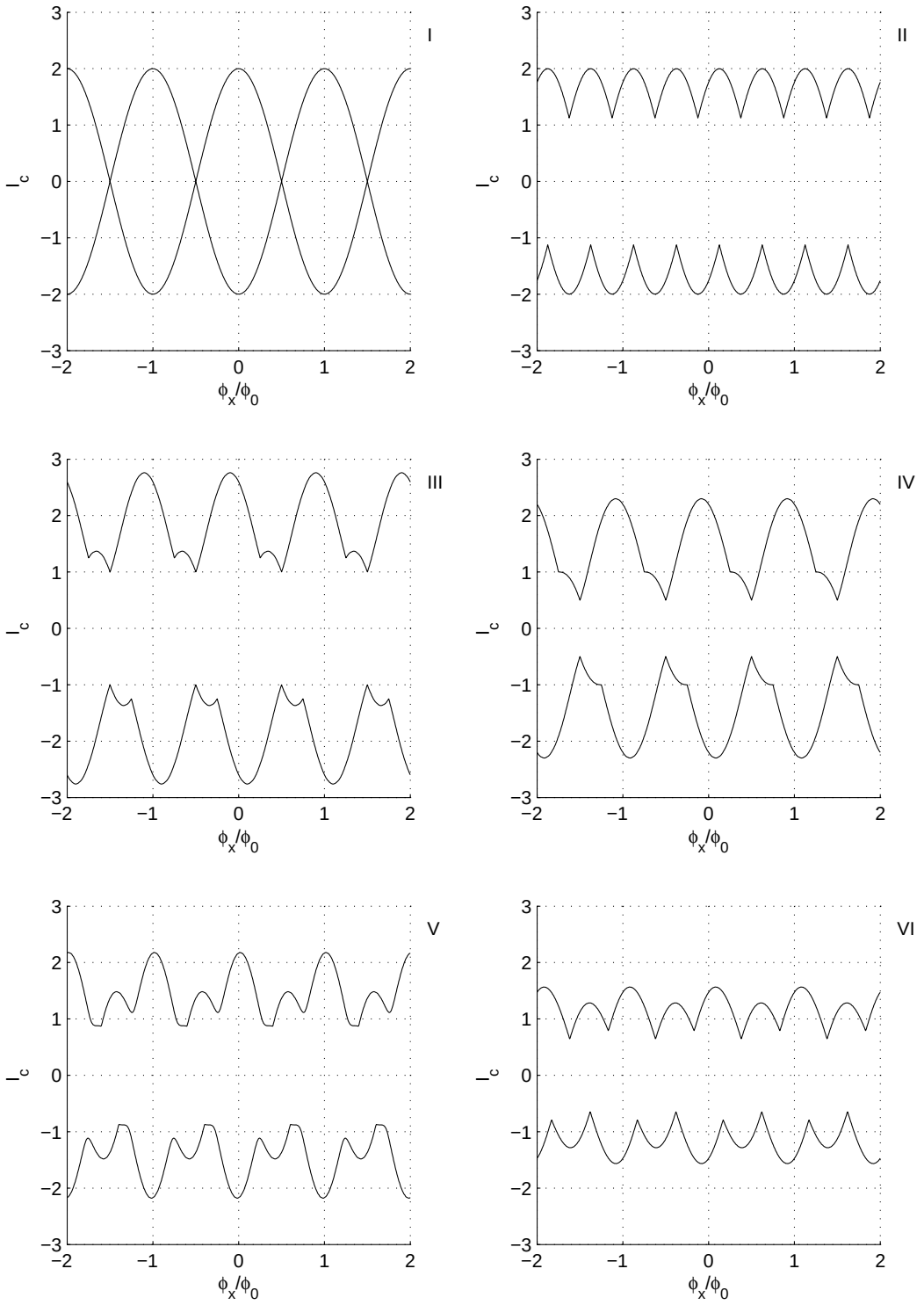

Figure 2.7: A few examples of I_c vs. ϕ patterns for dc-SQUIDs with different ratios of the 1^{st} and 2^{nd} harmonic.

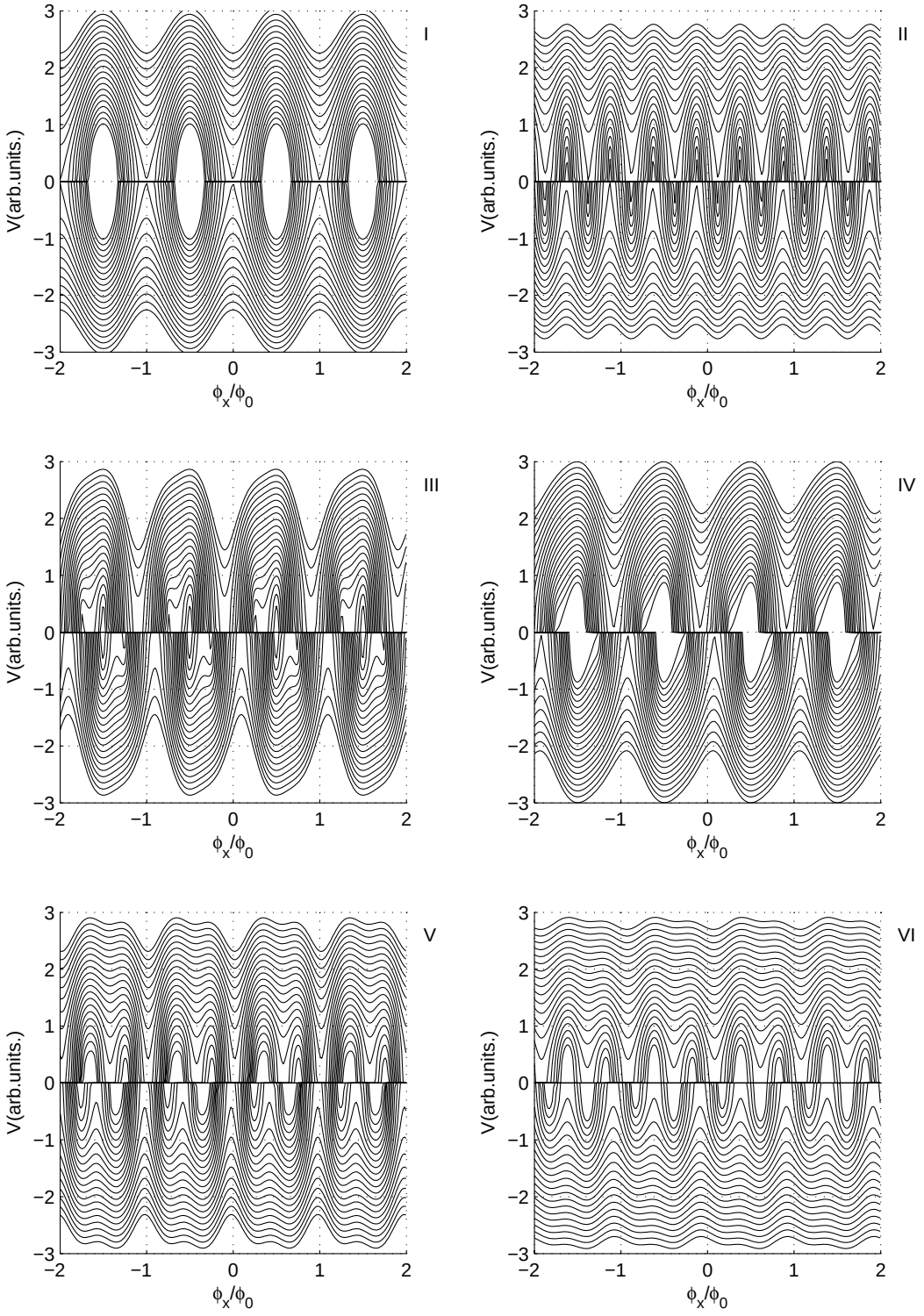

Figure 2.8: V vs. ϕ patterns. The parameters are the same as in figure 2.7, the patterns are plotted for $i = I/I_c = 1..3$.

Since λ_J depends on J_c it can vary with orders of magnitude even for junctions made of the same material; in YBCO junctions with $J_c = 10^2 - 10^7$ A/cm^2 it will varies between 100 nm-10 μm. λ_J is very important since it determines the "magnetic size" of the junction, when the width w of the junction is bigger than λ_J we need to take into account its self-field and screening currents when studying how the junction parameters are affected by an external magnetic field. In a junction with w smaller than λ_J the field will penetrate the junction uniformly, the junction is "short", whereas if $w > \lambda_J$ the flux dynamics of the junction starts to be important and the junction is "long".

Field suppression of the critical current:Distributed junctions

Unless a junction is very narrow its dynamics will be affected by even relatively moderate fields, this is true even for magnetically short junctions. In other words the junction has a certain width and the properties change as we move along the barrier if there is a field-gradient, it is *distributed* [27].
In general the current distribution is not uniform throughout the junction (unless perhaps the junction is very narrow; ~ 100 nm). Furthermore is also likely that there exist a few narrow "channels" with high conductance (this is a one very likely explanation for the lack of correlation between junction transparency and normal resistance which will be discussed later).
If we assume that the junction is magnetically short we do not need to take self-field effects into consideration and the dynamics can be described by a simple model [6]. We divide the junction into N pieces, each element being ΔX long and w thick and having a critical current $\delta I_c^n = J_c^n w \Delta x$ where the superscript denotes the element number. The presence of a magnetic field B creates a phase difference between each adjacent pair of elements since they are separated by a distance δz, the area of each loop being equal to $(2\lambda + t)\delta z \approx 2\lambda \delta z$s. When we move between two elements the phase will therefore change by an amount:

$$\delta\phi = \frac{2\pi(2\lambda + t)B}{\Phi_0}\Delta X \tag{2.39}$$

Hence, the total current through the junction is

$$I(\Phi) = \sum_{n=1}^{N}\sum_{k=1}^{\infty} \delta I_c^{n,k} \sin k(\delta\Phi + \theta) \tag{2.40}$$

where the inner sum is the CPR of the element and θ is the phase in the absence of a magnetic field. The critical current is equal to the maximum value of this sum with respect to Θ, if we assume that the CPR can be written $I^n(\Phi) = I_c^{I,n}\sin\Phi - I_c^{II,n}\sin 2\Phi$ we get

$$I_c(\Phi) = \max_{-\pi\leq\theta<\pi}\left[\sum_{n=1}^{N} I_c^{I,n}\sin(\delta\Phi + \theta) - I_c^{II,n}\sin 2(\delta\Phi + \theta)\right] \tag{2.41}$$

If only a first harmonic is present this can be written in the more familiar form (in the limit $\Delta x \to 0$)

$$I_c(\Phi)\left|\int_0^l w J_c(x)\exp(j\phi(z))dx\right| \tag{2.42}$$

which of course reduces to the familiar formula $I_{c0}|\sin(\pi\Phi/\Phi_0)|/|\pi\Phi/\Phi_0|$ when J_c does not change as we move along the boundary, i.e. we get the expression for the well-known Fraunhofer pattern.

[6]Note that the described model is just a extended version of the standard model of a distributed junction that can be found in e.g. [27], the generalization is needed in order to account for the possibility of an anomalous CPR.

A non-uniform J_c will change the shape of the pattern quite dramatically, this is especially true if a few channels with high conductance are included as seen in figure 2.9. Adding a 2^{nd} harmonic to the CPR modifies the pattern further effectively doubling the periodicity as can be seen in 2.10.
Note that the pattern in figure 2.9 is asymmetric with respect to zero-field. Lack of symmetry is usually attributed to flux trapping but can also be due to an unconventional CPR.

2.6 HTS Josephson Junctions

There are many ways to form Josephson junctions in HTS-materials, the most common types being Ramp junctions, Biepitaxial junctions, step-edge junctions and bicrystal junctions. Each technique has its advantages but unfortunately none of them can yet be used in large scale applications where a high degree of reproducibility is needed. Roughly speaking ramp junctions are used in applications such as digital electronics (RSFQ), whereas bicrystal junctions and biepitaxial junctions are used in research (one important exception being applications where only a single dc-SQUID is needed, here GBJJ are often used).

2.6.1 Grain Boundary Josephson Junctions

Even though it was one of the first techniques to be used for the study of the Josephson effect in HTS the grain boundary Josephson junction (GBJJ) is still an important tool. The technique itself is very simple, the idea is to create an artificial grain boundary which will act as a weak link. The method predates HTS since it can be used to study grain boundaries in many materials, it is used for many oxides including most perovskites.
Generally speaking a grain boundary can be considered as a plane of disorder within a single crystal where the degree of disorder is determined by the angle of misfit between the two sides of the plane [28]. The whole idea behind the GB technique is to introduce disorder in a controlled manner and in such a way as to have a well-controlled angle between the crystal axes in the electrodes.
Grain boundary junctions can be fabricated in several ways but here I will only discuss the bicrystal technique where the starting point is a substrate with an artificial grain boundary. The name stems from the fact that the substrate is made by joining two single crystals of different orientations as illustrated in fig 2.11. At the GB a various types of defects will be created in order to relax the lattice, at low angles edge dislocations will be created[29] but at higher angles other types of defects are also possible.
The real reason for the weak link behavior of the GB in YBCO can be found from one or several effects [29]

- Crystallographic misorientation
- Intergranular phases
- Impurities that gather at the GB
- Microcracks
- Changes in stoichiometry

It is very likely that the properties of the barrier will depend on the combined effect of several of these, the relative importance will also depend on the misorientation angle and the type of substrate used.

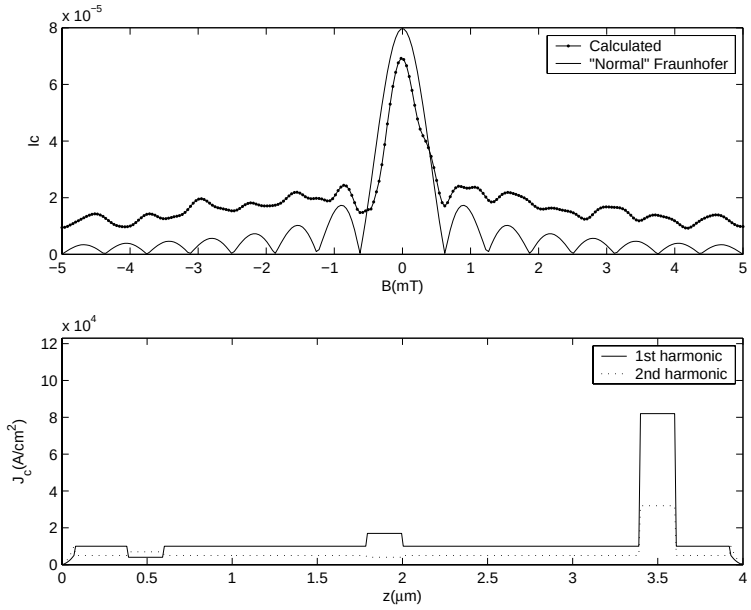

Figure 2.9: A so-called anomalous Fraunhofer pattern calculated using eq. 2.41. The current distribution of the 1^{st} and 2^{nd} harmonic respectively can be seen in the lower plot. Note that the pattern is slightly asymmetric with respect to zero field. The ”normal” Fraunhofer is calculated by assuming a J_c which is just the mean of the current distribution along the boundary.

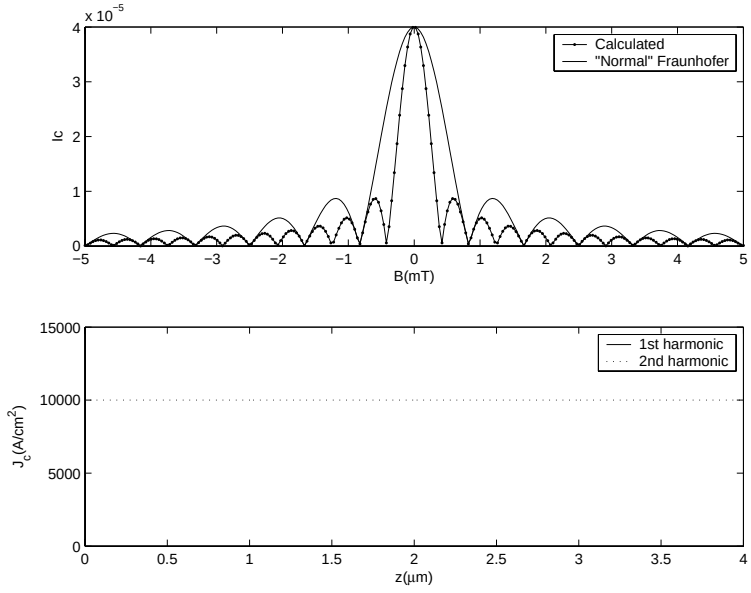

Figure 2.10: The anomalous Fraunhofer pattern when the junction is uniform and the CPR only contains a 2^{nd} harmonic.

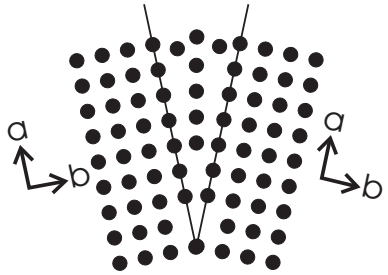

Figure 2.11: A schematic picture of a GB. The fusing of the crystals creates a region of disorder where the two lattices do not coincide.

Many materials are used as substrates for YBCO and most of them have also been used to make GBJJ. The most important materials are $SrTiO_3$ (STO), Y-ZrO_2 (YSZ), MgO, Al_2O_3(Sapphire), $LaAlO_3$ and LaSrAlTaO (LSAT). These are all oxides and most of them have a perovskite structure. It is well known that the transport properties of the GB vary depending on the substrate used, this further underlines the fact that misorientation angle alone can not explain the properties of the GB. Grain boundary junctions are classified as being of tilt (see fig. 2.12) or twist type according to how the bicrystal is formed [30]. Tilt junctions are formed when the crystal is rotated around an axis in the plane of the grain boundary and twist refers to a rotation perpendicular to the plane.

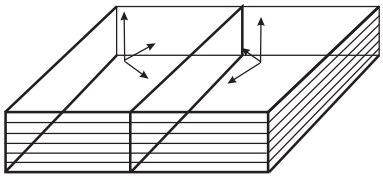

Figure 2.12: A [001]-tilt bicrystal.

2.6.2 J_c vs. angle for grain boundaries: d-wave effects

Even though this work is not concerned with power-applications it is interesting to note that it was when trying to understand why the critical current,J_c, [7] of polycrystalline samples were so much lower than one would have expected from measurement of the value of the gap-voltage that the concept of a d-wave order parameter was first established. In a famous work by Sigrist and Rice in 1992 [31] they showed that the critical current density of an all d-wave junction can be written

$$J_c = J_0(n_x^2 - n_y^2)_L(n_x^2 - n_y^2)_R \sin\varphi \tag{2.43}$$

where J_c is the maximum Josephson current density, φ is the difference in phase in the two electrodes, n_x and n_y are the projections of the unit vector $\mathbf{n}$ onto the crystallographic axes in the right(R) and left(L) electrode respectively. This result of course has very important implications

[7] The expression "critical current" is used in two different contexts. The critical current of a Josephson junction is the maximal supercurrent it can carry, the critical current of a film or bulk sample is the value of the current when the sample is starting to become resistive, either due to the self field becoming higher than the critical field or in a polycrystalline sample because the current carrying capabilities of the the grain boundaries have been exceeded

when trying to make for example cables that need to carry large currents. It tells us than in order to optimize the J_c of a polycrystalline sample we need to make sure that most of the GB are low-angle. It should however be pointed out that this result is not quite correct; according to eq. 2.43 the critical current should be zero in a 0°-45° junction (see figure 2.13) which is not the case (even though, as has already been mentioned, J_c is very low). As can be shown in a more detailed study[32], the reason for the discrepancy is that 2.43 does not consider transport through zero-energy Andreev states. Even though eq. 2.43 is phenomenological is agrees reasonably well with experiment on

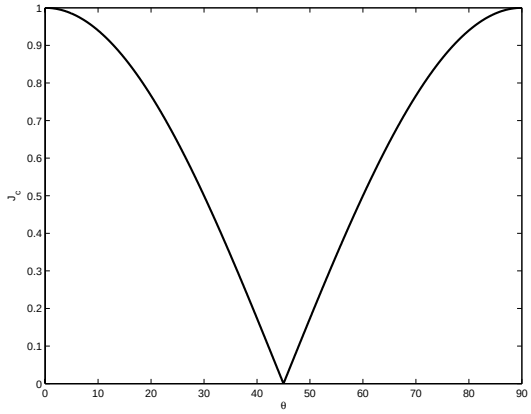

Figure 2.13: Critical current density as a function of angle for a 0-θ junction according to the Sigrist-Rice formula 2.43

single GB. This has been tested using the biepitaxial technique where it is possible to fabricate many junctions with different orientations on the same chip [33].

2.6.3 Excess current

Excess current is always a problem for HTS devices, and this is true also for bicrystal junctions. The physical mechanism behind excess current varies, it can be a consequence of a high-transparency barrier but also by ”defects” in form of pin-holes and micro-shorts. There are several effects which are usually attributed to excess current, not being able to completely suppress the critical current using an external magnetic field or microwave radiation and the slope of the normal branch of the IV curve not going through zero being the most common. The excess current is usually attributed to for example pinholes or other defects in the barrier. When working with high-angle junctions one has to be careful when interpreting the data. As was shown in the simulations the presence of a 2^{nd} harmonic in a non-uniform barrier affects the modulation in magnetic field and R_N is not always well defined. That said some of the supercurrent in our devices, both narrow and wide, is probably carried by excess current. It is possible that a better control of grain boundary could help reduce this problem

2.6.4 Andreev states

In 1994 Hu[34] suggested a novel mechanism for the creation of bound states in a superconductor with $d_{x_a^2-y_b^2}$ symmetry. Hu made the important observation that since the order parameter changes sign as one crosses a nodal direction states with essentially zero energy relative to the Fermi surface will be created [35]. Several experiments reported enhanced conductivity near zero bias voltage (a so-called ”zero-bias conductance peak”, ZBCP) in symmetric junctions and often this was explained

by scattering against magnetic impurities in the barrier. Hu was however able to show that the reason was more likely to be due to the existence of transport channels in which the current is carried by bound Andreev states.

Andreev transport is a well known phenomenon which is not unique to HTS materials. The basic process is quite simple if the wavefunction has an s-wave symmetry. An electron coming from a normal metal electrode impinges on a NS-boundary, if the energy of the electron is lower than the gap energy of the superconductor there are no available quasiparticle states on the S-side and the electron can not pass through the barrier, hence no current can flow. However, in an Andreev process the electron is reflected from the boundary as a *hole* which has an opposite momentum and charge, this means that a Cooper pair can be created in the superconducting electrode without violating charge- or energy conservation (since there is no restriction on the number of Cooper pairs that can exist below the gap). The net result of this process is therefore a charge transfer of 2e across the boundary, the whole process is illustrated in figure 2.14. The reason for the appearance of coherent Andreev states is that the electron- and hole-like wavefunctions, which have opposite electron momenta k_x (the momenta k_y parallel to the specular surface is conserved), can combine to form current carrying states. It can be shown that these states can form Andreev bands if phase dispersion is taken into account.

Andreev transport is not limited to transport across NS or IS interfaces but can also exist in for example SIS structures, in fact it turns out that if one calculates the current carried across such an interface by Andreev states the resulting equations will be identical to the Josephson equations 2.6 2.8; *Hence, all Josephson phenomena can be completely understood in terms of Andreev transport.* This picture is very useful when studying the Josephson effect in d-wave superconductors. The presence of bound states in Josephson junctions is often observed in symmetric junctions [36] but most systematic studies have used tunnelling spectroscopy where TRSB has also been observed[37].

In a high-angle HTS junction an Andreev process is much more complicated than in transport between two s-wave superconductors. The main difference stems from the fact that the wavefunction changes sign for certain quasiclassical trajectories. Figure 2.14 shows the orientation of the wavefunctions and the magnitude of the gap on both sides of the interface.

Here we will limit the discussion to the 0-45° case, for a more general discussion see the review by Löfwander [38]. Referring to figure 2.16 we see that the junction can be described as a SIS-structure.

A quasiparticle -hole- or electron-like- coming from the left electrode can give rise to Andreev transport, however since the phase changes by π when passing from one lobe to the next there will be *two* Andreev-levels, one with a effective phase $\tilde{\phi} = \phi$ (”zero-level”) and another with $\tilde{\phi} = \phi + \pi$ (”π-level). The current carried by the π-level will be a 2π-periodic function of the the phase, but will shifted by π with respect to the zero-level just as in so-called π-junctions which have a *negative* critical current. The net resulting current from both of these processes is π-periodic in phase and from the Josephson relations we see that the Josephson frequency doubles.

The model described above does not take noise and effects of disorder into account. The temperature dependence of the 2^{nd} harmonic differs from that of the 1^{st} which means that there can be a transition temperature where the transport starts to be dominated by the 2^{nd} harmonic, in Il’lichev et. al [24] found this temperature to be of the order of 20K. In realistic models of Andreev transport the roughness of the interface and scattering due to impurites and defects has to be taken into account. It can be shown [39] that this can drastically affect the transport properties of high-angle GBJJ. The main result of this analysis is that the Andreev processes giving rise to the 2^{nd} harmonic in the CPR can be suppressed if the quality of the interface is low.

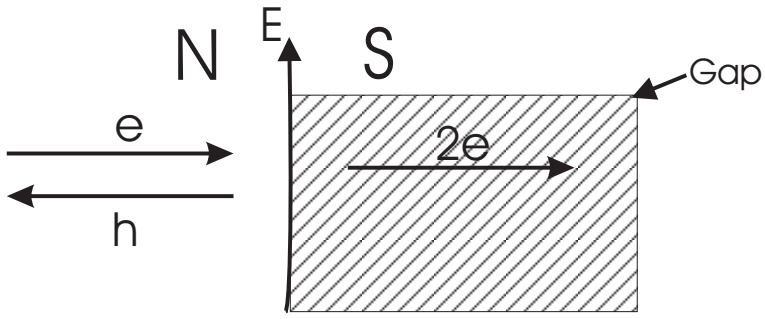

Figure 2.14: Conventional Andreev transport through a NS boundary when the superconducting wavefuntion has s-wave symmetry

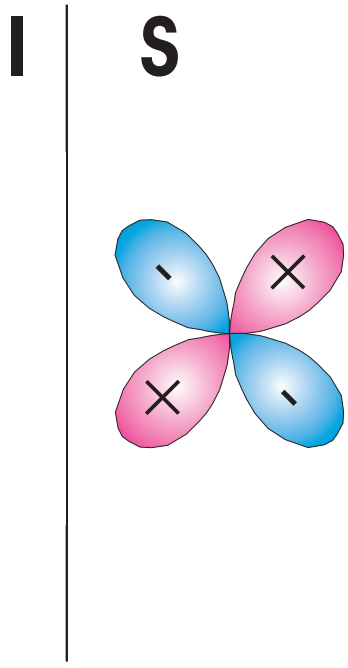

Figure 2.15: The formation of bound Andreev states at a specular interface between an insulator and a superconductor with $d_{x^2-y^2}$ symmetry, the superconducting electrode is rotated so that the node is normal to the interface.

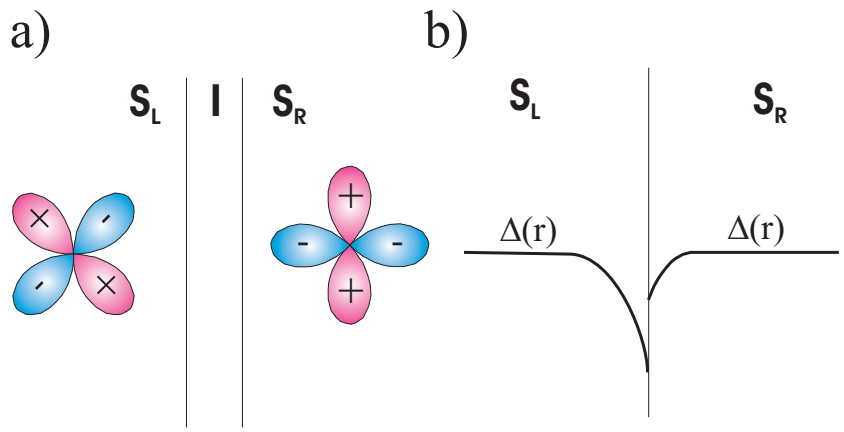

Figure 2.16: The formation of Andreev states in a specular 2-dimensional junction. a) The orientation of the wavefunction b) The magnitude of the gap

2.7 Some further properties of GBJJ

There are many other interesting phenomena that can take place in high angle grain boundaries, some of which are related to and sometimes also relevant in the devices studied in this thesis.
One important effect is that the vortex dynamics can be significantly altered at high-angle GB. For example can so-called *splinter vortices* form [40], these are unquantized but form pairs of that sum to Φ_0. This is still an active area of research and it is not completely clear how these affect the dynamics, their influence should however be insignificant as long as one is studying short junctions. Another effect related to this is the existence of spontaneous currents in grain boundaries [41], again this is an effect which is not that well understood experimentally even though it has been predicted in theoretical works.

2.8 Motivation for this work

The theories describing the effects of a d-wave order parameter in YBCO are still quite new. A number of convincing experiments have shown that the dynamics of Josephson junctions indeed are changed in high-angle junctions. The most dramatic change should occur for $0^\circ/45^\circ$-junctions since we then have a node-lobe transport. One important question has been what the effects of a strong 2^{nd} harmonic will have on the dynamics of devices. Another question is what happens when we make very small junctions on $0^\circ/45^\circ$ bicrystals, specifically what happens when the junction size is of the order of the characteristic length of the wiggling of the grain boundary. In addition, the high resistance of small junctions means that it is also possible to probe voltages close to and above the gap without using too much current. Hence, a number of problems have been studied:

- The influence of the 2^{nd} harmonic on the dynamics of dc-SQUIDs.
- Tunnelling spectroscopy of submicron $0^\circ/45^\circ$-junctions
- R_N, C, I_r and I_c of submicron junctions.

Chapter 3

Experimental

3.1 Device Fabrication

The devices used in this work were all fabricated using the same scheme. Since fabrication is somewhat outside of the scope of this work only a summary is given. A more detailed description can be found in Paper III.
The choice of substrate was dictated by the fact that is relatively easy to grow high-quality YBCO-films on STO and bicrystals with a well-defined GB is available. However, the material has one serious drawback which one needs to keep in mind; the dielectric constant of STO at low temperatures is huge. At 4.2K the low-frequency ϵ_r in a film is at least about 2000 [42] but can be as high as 20 000 in bulk samples. ϵ_r is also frequency-dependent. Due to the AC Josephson effect junctions and SQUIDs are ”natural” high-frequency devices and radiate energy, this means that a device can couple electromagnetically to a substrate which can for example result in resonances visible on the IV-curve.
All films used in this work were deposited using Pulsed Laser Deposition (PLD) on 5x5 mm^2 substrates, the film thickness was varied between 150-200 nm. The films were deposited under conditions which give a reasonable compromise between smoothness and critical temperature T_c (in general it is not possible to optimize both at the same time), T_c was usually close to 89K with a steep transition.
Using a rather thick film is crucial when fabricating small structures in any HTS material, the main problem one faces is oxygen out-diffusion and a thick film may reduce this problem. The electrodes leading to the structures can then function as oxygen reservoirs without being depleted themselves.

3.1.1 Lithography

There are many steps involved in the lithography, what follows is a short summary of the most important steps.

- A YBCO film is deposited on the substrate.
- A protective gold layer is deposited.
- The contacts, alignment marks and rulers are defined using e-beam lithography.

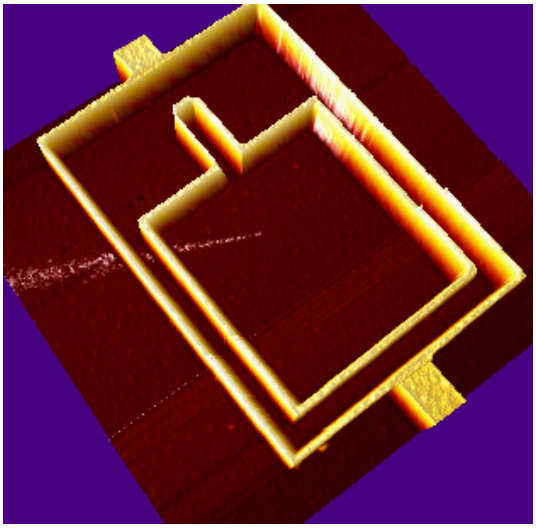

Figure 3.1: A large (20x15 μm^2) SQUID surrounding a smaller one (12x12 μm^2). The depicted area is 25x25 μm^2

- Since the GB is not located exactly in the middle of the chip the pattern needs to be adjusted. The deviation is measured using the rulers and the device drawings are changed accordingly.
- A layer of amorphous carbon (a-carbon) is deposited followed by a layer of NiCr.
- The pattern is defined in the NiCr using e-beam lithography.
- The pattern is transferred to the carbon layer.
- The YBCO is milled defining the final pattern. The etch rate of carbon is much lower than than of YBCO, the a-carbon essentially functions as a ”hard mask”.

A typical device fabricated using this technique can seen in figure 3.1. There are many steps in the fabrication procedure, it is however a quite reliable way to make very small structures in YBCO. 200 nm strips can be made with very high yield. It is possible to define even narrower structures but they are usually not superconducting, probably due to a low oxygen content.

3.1.2 Sample design

Designing SQUIDs for the types of experiments described in this thesis is not straightforward. The main problem is what loop size to use. Since we are not interested in maximizing the flux sensitivity we can make the loops rather small in order not to make the devices too sensitive to noise. On the other hand it is important to avoid having to use fields which are so high that they start to affect the properties of the junctions themselves. These considerations help us to determine that suitable sizes were 5x5, 10x10 and 15x15 μm^2.
Another important parameter when designing SQUIDs is the loop inductance. In our case it was important to keep the inductance as small as possible since the inductance directly influences the CPR of the SQUID. In order to be sure that the effect of the inductance could be safely neglected, we used the software package 3D-MLSI [43] to solve the problem numerically.

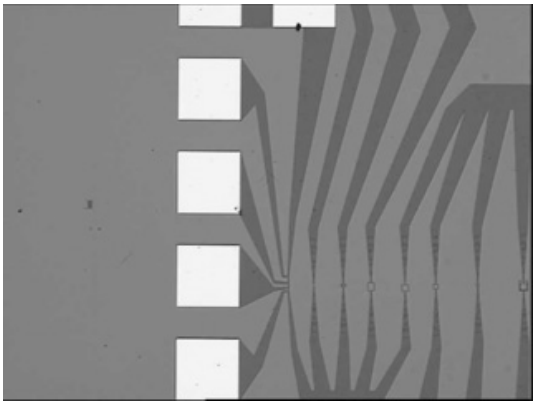

Figure 3.2: A 100x Micrograph showing a part of a typical chip. Various devices are shown including junctions and SQUIDs of various sizes.

There are about 20 structures (with 44 gold pads) on each sample, figure 3.2 shows a part of a typical chip. Even though the samples were designed with various measurements in mind, the basic design has stayed the same for the duration of this work. Junctions were fabricated with sizes ranging from 0.2-2 μm, the minimum size was set by technological limits whereas the maximum width was choosen in order to make sure that the junctions were in the short limit.

3.1.3 Considerations

From a physical point of view it is important to understand the effect of the fabrication on the properties of the film. Excessive heating at some point could for example lead to oxygen loss resulting in underdoped YBCO. Even though a device made from underdoped YBCO might work it would be hard to know how to interpret the results of a measurement since one would be probing properties which might differ a great deal from those of optimally doped YBCO.
We believe that the procedure outlined here, while cumbersome, helps to preserve the integrity of the the film. For the same reason other potentially useful techniques are not used, It is possible to fabricate very narrow structures using a Focused Ion Beam (FIB). However, in the case of FIB there are issues with possible gallium poisoning of the film, it is not fully understood how gallium doping affects the properties of YBCO. So for fundamental studies, it is best to avoid this technique.

3.2 The Measurement setup

All measurements have been done using a measurement setup known as ”RURIK” at Chalmers. The setup is always evolving as new equipment is added but the basic configuration has been the same for a few years.
The sample is glued to a chip holder and then wedge bonded using gold wires; the chip layout is designed so that it is always possible to do a 4-point measurement on each device. The chip holder is mounted on a dip stick which is then lowered into a magnetically shielded liquid helium cryostat. There is a small magnetic coil in the stick which makes it possible to apply fields of the order of 2 mT.
The devices are always current biased. It is very difficult to voltage bias HTS Josephson junctions and SQUIDs. Several attempts have been made but the end result is always inevitable: The

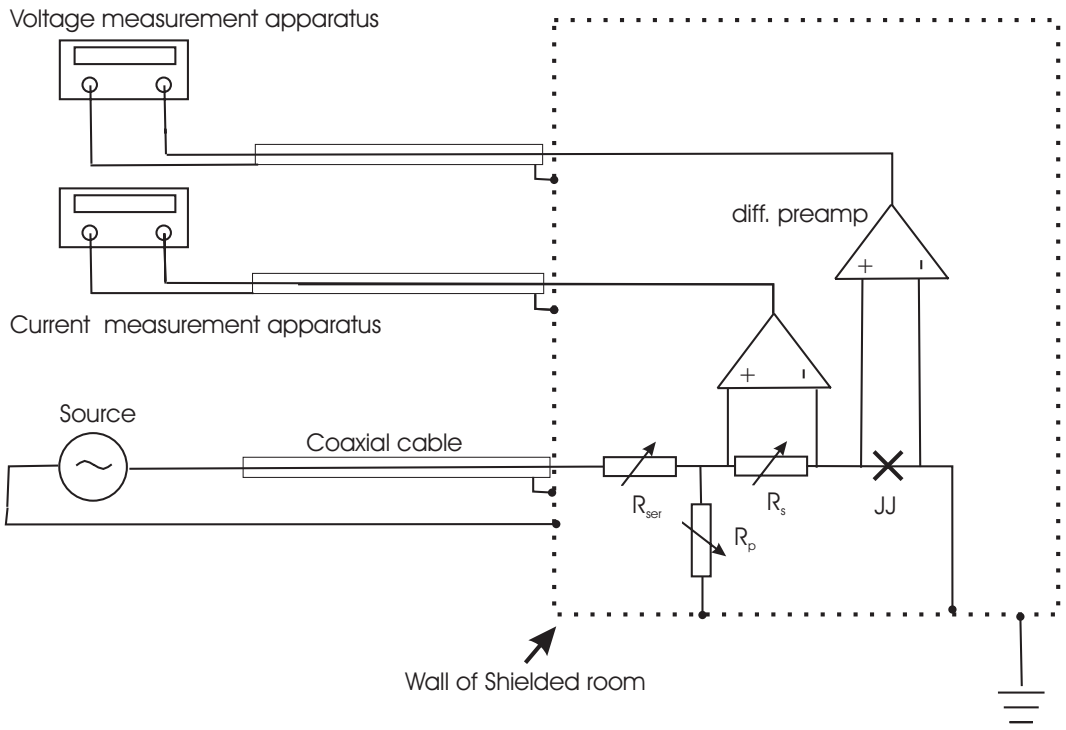

Figure 3.3: The RURIK system. R_{ser} is the series resistance, R_s the resistor used to measure the current, and R_p a resistor which can be connected in parallel with the Josephson junction.

destruction of the device under study. This is due to the fact that the load impedance of most of our devices is too low (often a few Ohms). Voltage biasing is only practical if the devices are relatively high-ohmic. This unfortunately means that it is difficult to directly compare the results with theoretical results since they almost always assume voltage bias. Even though this might seem trivial it is actually a big problem.
The biasing is done by connecting a series resistor, another smaller resistor is used in order to read out the current flowing through the circuit by measuring the voltage. Both current (indirectly) and voltage is measured by using two battery driven differential pre-amplifiers (Princeton Applied Research 5113). The cryostat and pre-amplifiers are kept in a EMI shielded room. The signals are then feed to various measurement devices located at the outside. The measurement electronics is powered from an insulating transformer which separates the measurement ground from the building ground. It also suppresses noise. All measurements are referenced to the wall of the shielded room. A schematic of the setup can be seen in figure 3.3.
The setup consists of

- 2 Princeton Applied Research 5113 differential pre-amplifiers
- 3 HP 3440A multimeters that are used for current-voltage characterization (”IV-measurement”)
- 1 Agilent 33220A arbitrary function generator used for biasing
- 1 Conductus LTC-21 temperature controller

- 1 Princeton Applied Research 5210 Lock-in amplifier
- 1 Yokogawa 7651 DC Source which is mainly used as current source for the magnetic coil
- 1 Fluke 3380A oscilloscope
- 1 National Instruments PCI-6052E 16-bit 333 kS/s Data Acquisition Card, used for various tasks such as IV-measurements, switching current measurements etc

Other types of equipment it also available when needed: Spectrum analyzers, microwave sources (up to 60 GHz), network analyzers etc. A fairly recent addition to the setup is an Oxford Heliox ^{3}He cryostat which can reach temperatures of 260 mK. The cryostat (in the form of a dip-stick) is kept in the shielded room, control-electronics and pumps are kept on the outside. The cryostat is magnetically shielded using a two-layer screen of Niobium and Cryoperm.
All control signals (temperature sensors, coil-bias, stepping motor for the Heliox etc) are routed through filtered feed-throughs.
When used correctly this setup is very suitable for low-noise measurements which is very important in the types of study presented in this theses. Access to a low-noise measurement setup is crucial in this type of experiments since in general the energy scale are set by the free energy of the junction/SQUID, the charging energy and the effective temperature (which is always higher than the bath temperature because of additional noise). An energy-conversion table can be found in Appendix A.

Chapter 4

Experimental Results

In this section I will summarize and comment on some the results that have been achieved over the past three years. Most of what will be discussed in this has been published and can be found in the appended papers. Whereas some of the papers are focused on the possible applications of the structures under consideration in quantum informatics, the focus of the discussion here will be on basic properties. A short discussion on one possible application can be found in chapter 6.
The results presented in this section were all obtained from 0°-45° YBCO grain boundary Josephson Junctions deposited on bicrystal STO substrates. All measurements were done at 4.2K unless stated otherwise.

4.1 Properties of High-Angle Junctions

The most basic measurement one can perform on a Josephson junction is a dc current-voltage characterization or "IV-curve". One can obtain a lot of information from an IV-curve and its derivative, the dynamic resistance dV/dI. It can directly give information about the energy spectrum of the various transport processes when plotted versus the voltage, a transport channel with an energy of for example 3 meV will appear as a dip in the dynamic resistance at 3 mV. Transport measurements can be considered to be a form of spectroscopy.
High-angle junctions often exhibit an IV-spectra rich with features. This is especially true in very narrow junctions since their high resistance means that the measurement often extends to voltages of the order of the gap voltage,Δ, which in the case of YBCO is about 25 meV. Hence, the BCS pair breaking voltage should be at $2\Delta \approx$50 meV in a YBCO junction. Indeed features in the spectra are often seen at around these values.
Figure 4.1 illustrates some typical I-V and dV/dI vs. V characteristics. They refer to a 0.2 μm wide 0°-45° junction at around 20 mK. The critical current can be seen to be about 400 nA but the normal resistance is not well defined. In conventional junctions R_N is defined as the resistance above the gap (which should be constant in a BCS superconductor) but here the dynamic resistance decreases up to about 50 mV (corresponding to 2Δ) and then it starts to increase. It varies between 150-250 Ω. There is no clear consensus on how to define R_N in HTS junctions. In most cases it is simply assumed that the dynamic resistance approaches some constant value at a current a few times I_c but this is not true in high-angle junctions.
There are also a number of peaks in the spectra shown in figure 4.1, these may be due to Multiple Andreev reflection (MAR) which occur at fractions of the gap voltage $2\Delta/n$[44]. MAR is not

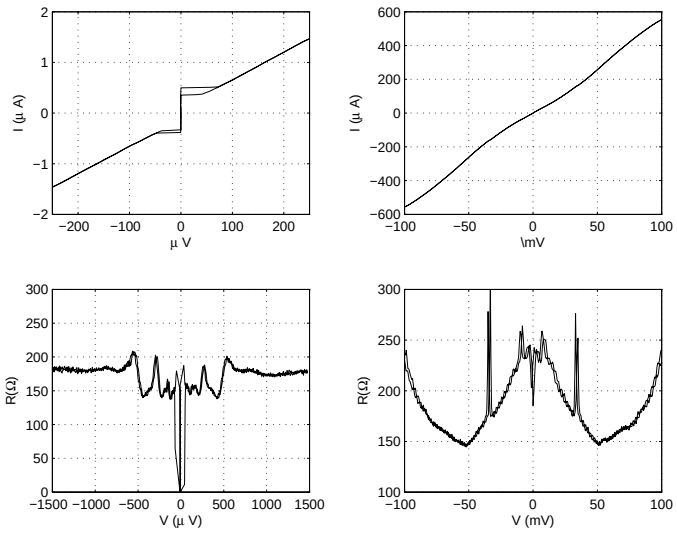

Figure 4.1: Current-Voltage characteristics and dynamic resistance for a 0.2 μm wide junction at 20 mK (the measurement was done using a dilution refrigerator).

expected to be present in 0°-45° junctions (in theoretical models MAR occurs in *symmetric* high-angle junctions) so probably their appearance means that some other angles are also present in the GB due to faceting.

4.1.1 Electrical Transport Properties

The submicron junctions that were investigated in our experiments generally exhibited a RCSJ-like behavior with a a hysteresis of about 30%. The capacitance was of the order of 50 fF.
The transport properties of GB junctions do not scale with the nominal width in a simple way. Figure 4.2 shows the critical current as a function of the nominal width for junctions ranging in size from 4 μm to 0.2 μm; at sizes below about 1 μm there is a crossover. This can be due to several effects

- The real width is different from the nominal. This can for example happen if the etching process causes the junctions to become rounded with sloped sides. AFM studies have however shown that the relative effect should be rather small unless the junction is extremely narrow, at sizes of 1 μm this effect should be negligible.
- Oxygen out-diffusion. It is not unreasonable to assume that there exist a thin ”dead layer” on the sides where the junction is not superconducting due to oxygen out-diffusion and disorder in the film. The thickness of this layer should not be directly related to the size of the features but the relative importance will of course increase as the junctions become more narrow.
- Defects/disorder, both natural and fabrication induced. Again, the relative importance will increase when the junction size decreases, it is however difficult to see why that would give a scaling behavior, the effect should be random.
- Finally, the barrier of the smaller junctions may be free from ’shorts’ - narrow channels of high transparency, which mainly govern the properties of the wider junctions. This possibility is supported by the fact that their I_c’s extrapolate to zero for the zero width as seen in fig.4.2.

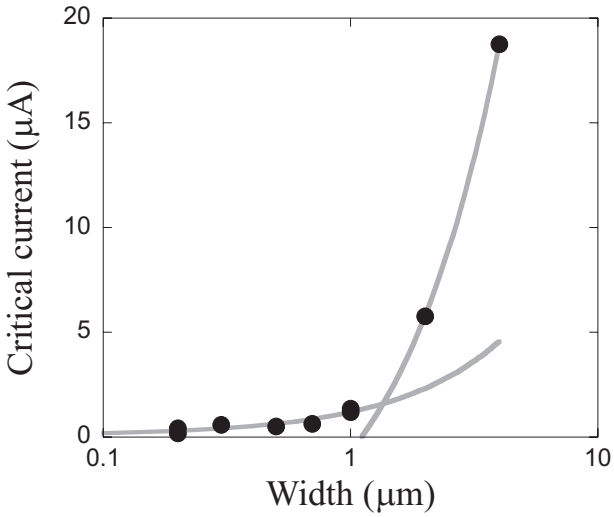

Figure 4.2: Critical current vs. width for a $0/45^\circ$ bicrystal measured at 4.2K

At the moment we do not fully understand the dependence of the Josephson current as a function of the width. It is however clear that the properties of small junctions can differ considerably from conventional GBJJ. A comparsison of the IV-properties can be seen in fig. 4.3.

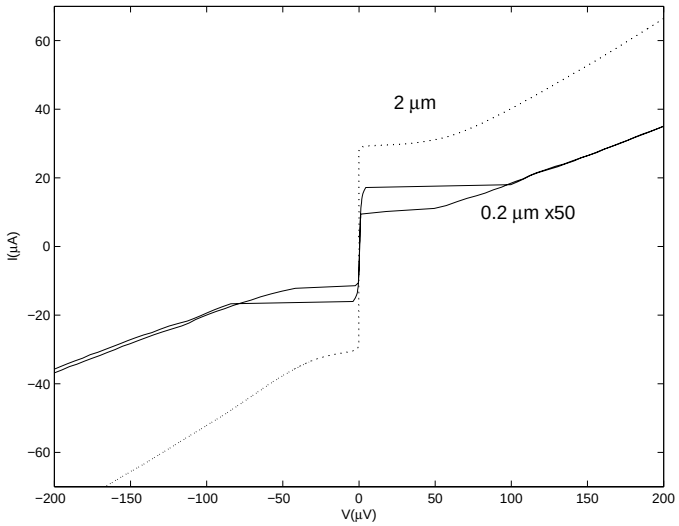

Figure 4.3: A comparison between SQUIDs with 0.2 μm and 2 μm (dotted line) junctions. The y-axis has for clarity been multiplied by 50 for the 0.2 μm SQUID.

It is interesting to note that even though there are some inconsistencies when comparing the parameters of wide and narrow junctions the behavior of junctions of equal width is relatively reproducible. A parameter spread of about 10% was observed on one chip. We also observed the usual scaling law $I_C R_N = j_c \rho_n \propto \sqrt{j_c}$ even when comparing junctions on different chips.

4.2 High-Angle Grain Boundary SQUIDs

The main focus of the work described in this thesis has been on dynamics of high-angle SQUIDs (with 0°/45° junctions). Here I will mainly discuss results from measurements on two SQUIDs (denoted SQ1 and SQ2), both from the same sample, which exhibit some interesting phenomena connected to the presence of a 2^{nd} harmonic. SQ1 and SQ2 are nominally identical symmetric SQUIDs with 15x15 μm loop-size and 2 μm wide junctions. The inductance was calculated using the software package 3D-MLSI [43] and was estimated to be 25 pH.

4.2.1 High-Field properties

Asymmetric high angle junctions generally exhibit a highly anomalous Fraunhofer pattern [45], (Elsev *et al.* [46] have actuality reported on a 0°/45° sample grown using Liquid Phase epitaxiy (LPE) showing a regular pattern, but this is an exception. The rest of their samples exhibited patterns similar to what is found in PVD-grown GBJJ) and this was also found to be the case with our samples.
Experimental data showing the high-field behavior of SQ1 and SQ2 can be found in figure 4.4 and 4.5. The shapes of the curves can be well described by a product of SQUID-oscillation and junction dynamics. Figure 4.4 is also a clear example of when the global maximum is *not* found in the centre of the pattern (i.e. even though there is a *local* maximum at $B = 0$, I_c is much higher in the "side-lobes"). The simple model described in section 2.5.3 can *not* explain this global minima which is sometimes observed in high-angle HTS Josephson Junctions. One explanation for this could be the presence of so-called π-facets in the boundary[45][47], this would have the effect of forming what is essentially small π-SQUIDs which in turn would induce negative currents (in the above model this could be modelled as regions with a negative J_c with only a 1^{st} harmonic present).
Figure 4.5 is a good example of a Fraunhofer pattern which is asymmetric with respect to zero-field but still is inversion-symmetric (see figure 2.9). This behavior can also be due to flux trapped in the SQUID-loop, but when that is the case some "hysteresis" is usually seen when sweeping the field back and forth. No such hysteresis was observed.

4.2.2 Low-field properties

Even though Josephson junctions are interesting, they do not usually reveal any information of the phase. The situation is analogous to optical experiments where some form of interference phenomena is used to study phase dependent effects. As has already been pointed out dc-SQUIDs are interferometers by their very nature and it is therefore natural to use them to study the superconducting phase.
Here we will not dwell on things that are usually discussed in conjunction with SQUIDs, parameters like modulation depth are important when using SQUIDs in applications (for example as sensitive magnetometers) but are not really relevant in our case.
Figures 4.6-4.8 show experimental data for SQ1 and SQ2. The shape of the CPR has been estimated by extracting the parameters[1] using the I_c-B characteristics.
Using the fitting parameters obtained from the experimental data one can plot the CPR of the individual junctions. In figure 4.9 the calculated CPR from 4 junctions (from SQA and SQB) is

[1]The parameters were estimated using a non-linear least-square fit using the optimization toolbox in Matlab, a straightforward Fourier analysis is unfortunately difficult to use on the real experimental data. See appendix B

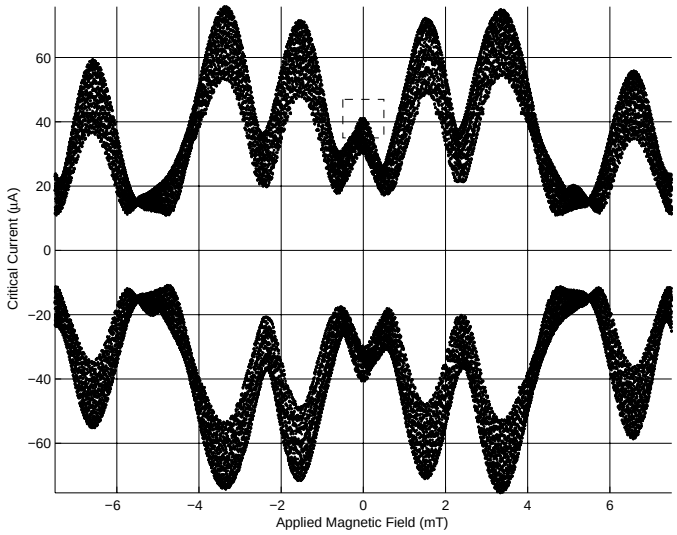

Figure 4.4: The critical current vs. magnetic field for SQ1 with 2μm wide junctions.

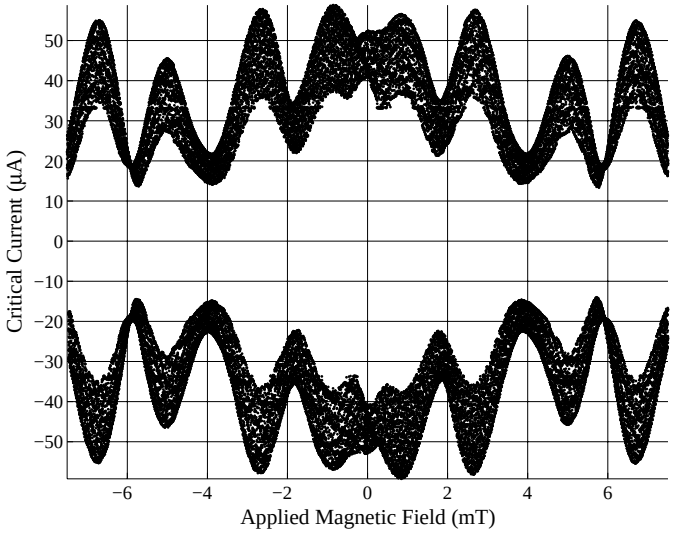

Figure 4.5: The critical current vs. magnetic field for SQ2.

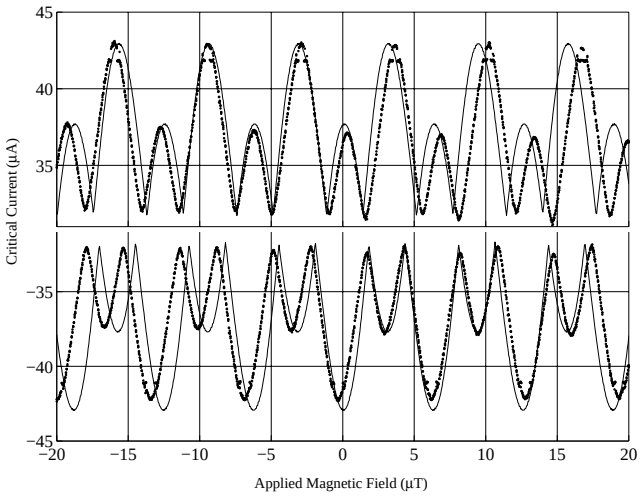

Figure 4.6: The critical current vs. magnetic field for SQ1. *Dotted line:* Experimental data *Solid line:* Theoretical fit. The fitting parameters are: $I_{c1}^{I} = 9$ μA, $I_{c2}^{I} = 0.3$ μA, $I_{c1}^{II} = 3.7$ μA and $I_{c2}^{II} = 22.7$ μA. Note that the y-axis scale does not start at zero.

shown, Note that the junctions which have a substantial 2^{nd} harmonic in their CPR exhibits an almost π-periodic behavior.
In order to be able to fit the data using our simple model one sometimes has to assume the presence of a quite substantial excess current, the amount varies between samples but can be as much as 50% of the supercurrent. Though somewhat discouraging this is not unreasonable, excess currents of this order are frequently observed also in lower angle GBJJ.

SQUIDs with narrow junctions

One thing which does *not* follow from the calculations is that the dynamics of SQUIDs with narrow width (about 1 μm) does not exhibit any sign of higher harmonics in the CPR (see fig 4.10).
This somewhat surprising fact could have several explanations, it could for example be due to the effects of disorder of scattering. This could happen if the smaller junctions have a higher degree of disorder at the interface due to fabrication induced damage our oxygen out-diffusion. Another reason could be that the wiggling/facetting of the GB just happened not to be close enough to 0/45° in the samples we have investigated, this is not a very likely explanation. One reason for the difference could be that there *is* a 2^{nd} harmonic in the CPR but that we can not detect it; if the washboard has a shape where the ”extra” wells (responsible for the higher harmonics in the I_c-B and V-B characteristics) are so shallow that the phase can escape due to thermal excitation the effects of a 2^{nd} harmonic would be difficult to detect. Or in other words, the reason why you do not see a effect on the dynamics is the small critical current in narrow junctions. In order to see if that is indeed the case one have to compare the Josephson energy of the 2^{nd} harmonic , E_J^{II}, which approximately gives the height of the extra ”hump” with the thermal energy. Such calculations have been done and seem to indicate that this could be the reason for the difference between SQUIDs with large- and small junction. However, the models are rather rough and can only give order-of-magnitude estimates and since we do not yet know if the extracted values of I_c^I and I_c^{II} are correct we can not say for sure.

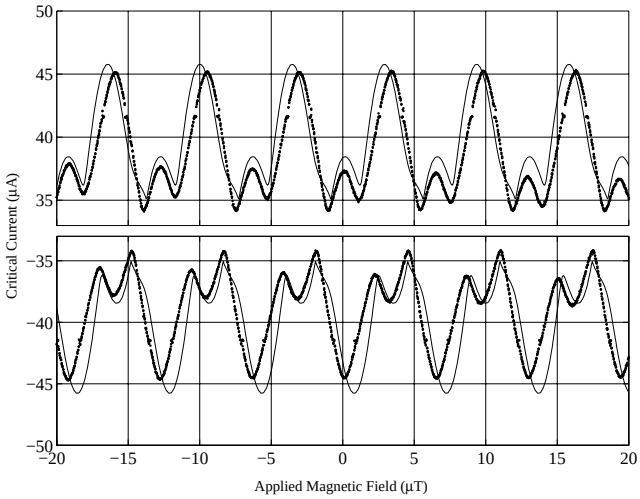

Figure 4.7: The critical current vs. magnetic field for a SQ2. *Dotted line:* Experimental data *Solid line:*. Fitting parameters are: $I_{c1}^{I} = 7.8\ \mu$A, $I_{c2}^{I} = 3.0\ \mu$A, $I_{c1}^{II} = 5.3\ \mu$A and $I_{c2}^{II} = 4.3\ \mu$A

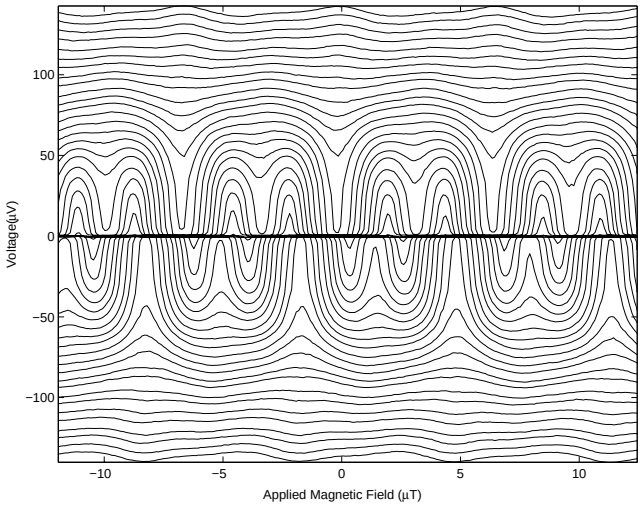

Figure 4.8: The voltage modulation at different bias currents for SQUID SQ1.

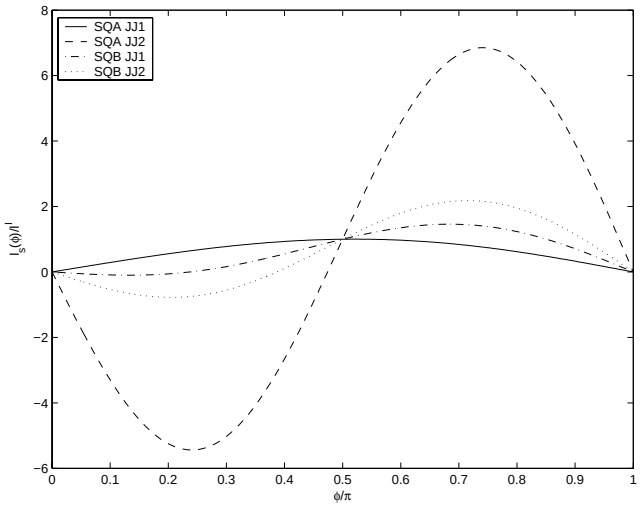

Figure 4.9: CPR for the junctions in SQA and SQB normalized to I^I.

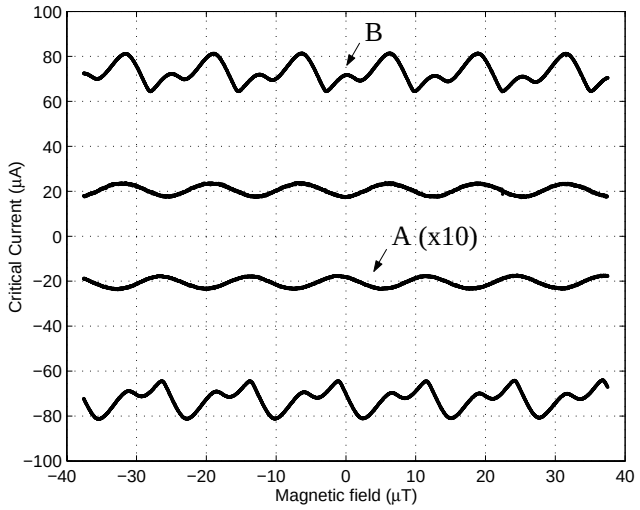

Figure 4.10: A comparison of the dynamics of a SQUIDs with wide (A) and (B) narrow junctions, both SQUIDs have the same area. The junction sizes are 2/2 μm and 0.3/0.2 μm respectively. Note that the two curves are drawn in different scales in order to be able to compare them.

Chapter 5

Discussion

The experimental results and the numerical calculations presented in this thesis are in good agreement. Models based on the assumption of a strong 2^{nd} harmonic in 0/45° junctions can be used to explain several phenomena

- Strongly non-sinusoidal modulation and effective doubling of the period of dc-SQUIDs.
- The reason for anomalous Fraunhofer patterns.
- The relative shift of the positive and negative period of the modulation.
- The fact that the maximum critical current of a dc-SQUIDs is shifted from zero magnetic field.

However, there are several observed phenomena which can not be explained

- Why the global maximum of the critical current of junctions is not found at zero-field.
- The discrepancy between the barrier transparancy calculated from R_N and the value one gets from comparing the ratio I^{II}/I^{I}.
- Why most phenomena resulting from a 2^{nd} harmonic are not observed in SQUIDs with narrow ($< 1\mu$m) junctions

Especially the last point is very important, even though there are several possible solutions more experiments are needed before this point can be settled.

5.0.3 A multi-channel transport model

The results one obtains from transport measurements of GB junctions quite often contradict each other. They seem to point in different directions with regard to things like barrier transparency, GB structure etc. One example is that one can calculate the transparency of the barrier by using the ratio of the 1^{st} and 2^{nd} harmonic present in a junction[24], however comparing this data to what one estimates from for example the resistivity of the junction (using e.g. the BTK-model) which can also be used to calculate the transparency, the result can differ by several orders of magnitude.
Many, but not all, of these difficulties can be overcome if one assumes that several independent transport channels can exist in the junction, each one having a certain conductance. These channels

can be either structural (due to the wiggling/facetting of the GB) or perhaps energy dependent (different channels dominate depending on the voltage over the junction) This obviously explains the co-existence of the 1^{st} and 2^{nd} harmonics in 0/45° junction (which of course could also be due to a *transport channel* with a CPR which contains a large 2^{nd} harmonic as in point contacts).
It is well known that the microstructure of the GB is important for the transport properties of GBJJ, but the importance of the interface increases when dealing with high-angle junctions since wiggling of the GB can cause deviations from the desired geometry. While preserving the total misorientation angle, an uneven boundary affects the relative orientation of the grains with respect to its plane. For example, a nominally 0/45° junction may locally become 22.5/22.5° or 10/35°. The symmetry conditions of node-to-lobe tunnelling leading to the cancellation of the first harmonic, would be locally violated.
Under certain conditions imperfections of the barrier may perhaps form high-transparency channels, which will effectively shunt ”high-angle parts” of the junction simply because the conductance of low-angle channels can be several orders of magnitude higher. In wide junctions (many experiments use GB junctions which are wider than 10 μm) the transport properties will be given by the average properties of all the channels in the GB, therefore effect of low-conductance channels will be washed out.
Some of the junctions used in the experiments described in this theses are very narrow, down to about 200 nm. Since the wiggling of the GB is of the order of 50-200 nm these junctions should in principle probe a *single* channel. However, the fact that they do exhibit such a complicated behavior could be an indication that the transport properties are also affected not only by the wiggling but also by the facetting. From TEM-studies we know that the typical sizes here are of the order of a few nanometers, which is of the same order as the coherence length in YBCO. Whether or not facetting on this small scale has to be taken into account is an open question. The fact that we *do* see a clear change in properties as the ”macroscopic” GB-angle is changed suggests that we do have a high degree of control despite all of this. To the best of my knowledge no theoretical model exists which can explain exactly how the the microscopic properties of a grain-boundary are manifested in the transport properties.

5.0.4 Submicron junctions

The fact that it is possible to fabricate submicron YBCO junctions with a relatively high degree of reproducibility opens up interesting possibilities. The parameters of these junctions indicates that it might be possible to observe quantum behavior such as level splitting at low enough temperatures. The main question at this point is why we do not see any indication of a 2^{nd} harmonic in the CPR when studying SQUIDs with submicron junction and whether or not this is a result of intrinsic properties. This issue needs to be resolved in order to be able to understand if it is possible to use these junctions in quantum processing. Note however that the direct measurement of the CPR performed in [24] was done on submicron junctions and that data is quite similar to what has been shown in this work, even though that work was done on symmetric 22.5°/22.5° junctions.

Chapter 6

Summary and Outlook

The dynamics of high-angle YBCO SQUIDs and junctions is a very complicated phenomenon which we do not fully understand. As has been shown in this thesis one can get a wide variety of behaviors even in structures on the same chip. Even with very sophisticated models it is difficult to predict how a structure will behave since we do not know how to control the properties of the grain boundary very well. It is possible that more reproducible fabrication technologies are needed before we can get the complete picture. In the meantime there are many interesting basic experiments that can be done using the bicrystal technique.

6.1 Future Experiments

Even though we are starting to understand some of the properties of high-angle GBJJ more experiments are needed. Here I will just mention a few areas where more data are needed.

- Temperature dependence of the dynamics of high-angle dc-SQUIDS. The experiments are quite complicated since flux dynamics become important when the temperature starts to change. It is sometimes difficult to determine if an effect is due to temperature or thermally activated flux motion.

- More data are needed to completely characterize the dynamics of SQUIDs with small junctions. These experiments should be performed at low temperatures in order to have $E_J \gg k_B T$.

- The relative amount of 1^{st} to 2^{nd} harmonic of the Josephson current has been calculated from experimental data using simple models. It should be straightforward to repeat these measurement on specially prepared samples where it is possible to cut the SQUID-loop and measure the individual junctions. This way it will be possible to check if the calculated fitting parameters agree with the measured parameters of each junction.

- It would be interesting to repeat the measurements using a different superconductor. Electron- and hole doped materials would be especially interesting to try.

6.1.1 Implications of this work

An important point of this work is that what has been studied are ”ordinary” dc-SQUIDs and junctions; it is the wiggling and facetting of the GB which causes the effects of a 2^{nd} to become clear. From what we know of the properties of the GB it is likely that some of the effects studied here might also exist to some extend in more conventional GB junctions without direct tunnelling into the node. The effects of an unconventional CPR are often undesirable since they will for example reduce the sensitivity of a SQUID-magnetometer. Another interesting question is if some of the existing theory for dc-SQUIDs needs to be modified in order to account for these effect. An obvious question which has not been studied in this work is what happens to the noise spectra of junctions and SQUIDs when the CRP is non-sinusoidal. This is only one of many possible implications.

6.2 A HTS Qubit?

The unconventional CPR of $0/45^\circ$ junctions could potentially be used to create building blocks for quantum computers[48]. In order to create a qubit one needs a two-level system with the following properties

- Quantum coherence should be upheld for a time long enough to perform a number of operation.
- It should be possible to isolate the qubit during the operation. The system has to be isolated from the environment in order to prevent decoherence.
- There must be a way to turn the interaction with the environment on and off in order to perform a quantum measurement.
- It should be possible to prepare the system in a known state
- There should be a way to couple many qubits together
- In order to build a real computer there must be way to fabricate and control thousands of qubits.

It is straightforward to show that YBCO dc-SQUIDs with $0/45^\circ$ junctions such as the ones described in this thesis fulfill at least some of these requirements [49]. The energy potential of an asymmetric $0/45^\circ$ dc-SQUID has a double well shape which can be manipulated with the help of an external magnetic field. It should be possible to prepare the system in a known single state. It can also be shown that all the usual gate-operations can be performed using microwave pulses[50].
More studies are needed before we can establish if a ”d-wave qubit” is indeed possible. However the prospects are promising enough to warrant further effort in this field.

Chapter 7

Acknowledgements

Experimental physics is always a collaborative effort and the results presented in this thesis are the combined effort of many people. I would like to thank Alexander Ya. Tzalenchuck and Serge Charlebois, without them none of the work presented here would have been possible.
Evgueni A. Stepantsov has helped us many times and deposited many of the films used in this study.
An invaluable person in our work is our technician Staffan Pehrson who has helped us many times and built much of our equipment.
As a Ph.D student I would not be able to do much without the support and help from my supervisor Floriana Lombardi and my examiner Tord Claeson. Your efforts are greatly appreciated.
Much of the theory presented in this thesis has been developed by our our collaborators Alexander Zagoskin and Mohammad H.A. Amin, both at D-Wave Systems.
I have also received helped from many other people of whom I can only mention a few: Michael Tarasov, Alexei Kalabukov and Philippe Komissinski have all helped me many times.

Finally I would like to thank all members of the Quantum Device Physics Laboratory at Chalmers.

Between 2000-2003 my supervisor was Professor Zdravko Ivanov who passed away on May 20th, 2003. He was a great source of inspiration and knowledge; both as a scientist and as a person.

Bibliography

[1] J.G. Bednorz and K.A. Muller. Possible high-T_c superconductivity in the Ba-La-Cu-O system. *Zeitschrift fur Physik B (Condensed Matter)*, 64(2):189–93, 1986.

[2] J. Moreland, L.F. Goodrich, J.W. Ekin, T.E. Capobianco, A.F. Clark, A.I. Braginski, and A.J. Panson. Josephson effect above 77 K in a YBaCuO break junction. *Applied Physics Letters*, 51(7):540–1, 1987.

[3] J Bardeen, J.N Cooper, and J.R. Schrieffer. *Phys. Rev*, 108:1175, 1957.

[4] M. Tinkham. *Introduction to Superconductivity*. McGraw-Hill, 1996.

[5] D.A. Wollman, D.J. Van Harlingen, W.C. Lee, D.M. Ginsberg, and A.J. Leggett. Experimental determination of the superconducting pairing state in YBCO from the phase coherence of YBCO-Pb DC SQUIDs. *Physical Review Letters*, 71(13):2134–7, 1993.

[6] C.C. Tsuei and J.R. Kirtley. Pairing symmetry in cuprate superconductors. *Reviews of Modern Physics*, 72(4):969–1016, 2000.

[7] J. Mannhart and H. Hilgenkamp. Wave function symmetry and its influence on superconducting devices. In D.H.A. Rogalla, H.; Blank, editor, *Applied Superconductivity 1997. Proceedings of EUCAS 1997 Third European Conference on Applied Superconductivity*, pages 1–6 vol.1, Bristol, UK, 1997. Institute of Physics Publishing.

[8] D. Winkler. Superconducting analogue electronics for research and industry. *Superconductor Science and Technology*, 16:1583–1590, 2003.

[9] B.D Josephson. Possible new effects in superconductive tunneling. *Physics Letters*, 1(7):251–253, 1962.

[10] R Feynman, R Leighton, and M Sands. *The Feynman Lectures on Physics*. Addison-Wesley, 1965.

[11] K.K. Likharev. *Dynamics of Josephson Junctions and Circuits*. Gordon an Breach Science Publishers, 1986.

[12] D. Winkler, Y.M. Zhang, P.A. Nilsson, E.A. Stepantsov, and T. Claeson. Electromagnetic properties at the grain boundary interface of a $YBa_2Cu_3O_{7-\delta}$ bicrystal josephson junction. *Physical Review Letters*, 72(8):1260–3, 1994.

[13] M. Sigrist and T.M. Rice. Unusual paramagnetic phenomena in granular high-temperature superconductors-a consequence of d-wave pairing? *Reviews of Modern Physics*, 67(2):503–13, 1995.

[14] T Löfwander, V. S. Shumeiko, and G. Wendin. Time-reversal symmetry breaking at josephson tunnel junctions of purely d-wave superconductors. *manuscript*, 2000.

[15] M.H.S. Amin, A.N. Omelyanchouk, and A.M. Zagoskin. Mechanisms of spontaneous current generation in an inhomogeneous d-wave superconductor. *Physical Review B (Condensed Matter and Materials Physics)*, 63(21):212502–1, 2001.

[16] G.E. Blonder, M. Tinkham, and T.M. Klapwijk. Transition from metallic to tunneling regimes in superconducting microconstrictions: excess current, charge imbalance, and supercurrent conversion. *Physical Review B (Condensed Matter)*, 25, 1982.

[17] G.E. Blonder, M. Tinkham, and T.M. Klapwijk. Transition from metallic to tunneling regimes in superconducting microconstrictions: excess current, charge imbalance, and supercurrent conversion. *Physical Review B*, 25, 1982.

[18] J R Waldram. *Superconductivity of Metals and Cuprates*. IOP Publishing, 1996.

[19] J.C. Gallop. *SQUIDs, the Josephson Effects and Superconducting Electronics*. IOP Publishing, 1991.

[20] S.-K. Yip, O.F. De Alcantara Bonfim, and P. Kumar. Supercurrent tunneling between conventional and unconventional superconductors: a ginzburg-landau approach. *Physical Review B (Condensed Matter)*, 41(16):11214–28, 1990.

[21] Sungkit Yip. Josephson current-phase relationships with unconventional superconductors. *Physical Review B (Condensed Matter)*, 52(5):3087–90, 1995.

[22] A.M. Zagoskin. The half-periodic josephson effect in an s-wave superconductor-normal-metal-d-wave superconductor junction. *Journal of Physics: Condensed Matter*, 9(31):419–26, 1997.

[23] H. Arie, K. Yasuda, H. Kobayashi, I. Iguchi, Y. Tanaka, and S. Kashiwaya. Josephson tunneling of anisotropic high-T_c d-wave junctions with tilted ab-plane $YBa_2Cu_3O_{7-y}$ electrodes. *Physical Review B (Condensed Matter)*, 62(17):11864–71, 2000.

[24] E. Il'ichev et al. Degenerate ground state in a mesoscopic $YBa_2Cu_3O_{7-x}$ grain boundary josephson junction. *Physical Review Letters*, 86(23):5369–72, 2001.

[25] M.H.S. Amin, A.Yu. Smirnov, A.M. Zagoskin, T. Lindstrom, S.A. Charlebois, T Claeson, and A.Y. Tzalenchuk. Silent phase qubit based on d-wave josephson junctions. *Cond-Mat/0310224*, 2003.

[26] S.K. Tolpygo and M. Gurvitch. Critical currents and josephson penetration depth in planar thin-film high-T_c josephson junctions. *Applied Physics Letters*, 69(25):3914–16, 1996.

[27] Alan M Kadin. *Introduction to Superconducting Circuits*. John Wiley & Sons, 1999.

[28] P.E. Flewitt and R.K. Wild. *Grain Boundaries-Their Microstructure and Chemistry*. Wiley, 2001.

[29] José A. Alarco. *Grain Boundary Structure of YBCO High-Tc Superconductors*. PhD thesis, Göteborg University, 1994.

[30] H. Hilgenkamp and J. Mannhart. Grain boundaries in high-T_c superconductors. *Reviews of Modern Physics*, 74(2):297–659, 2002.

[31] M. Sigrist and T.M. Rice. Paramagnetic effect in high-T_c superconductors-a hint for d-wave superconductivity. *Journal of the Physical Society of Japan*, 61(12):4283–6, 1992.

[32] M.B. Walker and J. Luettmer-Strathmann. Josephson tunneling in high-T_c superconductors. *Physical Review B (Condensed Matter)*, 54(1):588–601, 1996.

[33] F. Lombardi, E. Tafuri, F. Ricci, F.M. Granozio, A. Barone, G. Testa, E. Sarnelli, J.R. Kirtley, and C.C. Tsuei. Intrinsic d-wave effects in $YBa_2Cu_3O_{7-\delta}$ grain boundary josephson junctions. *Physical Review Letters*, 89(20):207001–1, 2002.

[34] Chia-Ren Hu. Midgap surface states as a novel signature for $d_{x_a^2-x_b^2}$-wave superconductivity. *Physical Review Letters*, 72(10):1526–9, 1994.

[35] M. Fogelström, D. Rainer, and J.A. Sauls. Tunneling into current-carrying surface states of high-T_c superconductors. *Physical Review Letters*, 79(2):281–4, 1997.

[36] L. Alff, A. Beck, R. Gross, A. Marx, S. Kleefisch, Th Bauch, H. Sato, M. Naito, and G. Koren. Observation of bound surface states in grain-boundary junctions of high-temperature superconductors. *Physical Review B (Condensed Matter)*, 58(17):11197–200, 1998.

[37] L. H. Greene, M. Covington, M. Aprili, E. Badica, and D. E. Pugel. Observation of broken time-reversal symmetry with andreev bound state tunneling spectroscopy. *Physica B*, 280(1-4):159–64, 2000.

[38] T. Löfwander, V.S. Shumeiko, and G. Wendin. Andreev bound states in high-T_c superconducting junctions. *Superconductor Science and Technology*, 14(5):R53–77, 2001.

[39] Yu.S. Barash. Quasiparticle interface states in junctions involving d-wave superconductors. *Physical Review B (Condensed Matter)*, 61(1):678–88, 2000.

[40] R.G. Mints, I. Papiashvili, J.R. Kirtley, H. Hilgenkamp, G. Hammerl, and J. Mannhart. Observation of splintered josephson vortices at grain boundaries in $YBa_2Cu_3O_{7-\delta}$. *Physical Review Letters*, 89(6):067004–1, 2002.

[41] F. Tafuri, J.R. Kirtley, F. Lombardi, and F.M. Granozio. Intrinsic and extrinsic d-wave effects in $YBa_2Cu_3O_{7-\delta}$ grain boundary josephson junctions: implications for pi circuitry. *Physical Review B (Condensed Matter and Materials Physics)*, 67(17):174516–1, 2003.

[42] E.J. Tarte, P.F. McBrien, J.H.T. Ransley, R.H. Hadfield, E. Inglessi, W.E. Booij, G. Burnell, M.G. Blamire, and J.E. Evetts. Capacitance as a probe of high angle grain boundary transport in oxide superconductors. *IEEE Transactions on Applied Superconductivity 2000 Applied Superconductivity Conference, 17-22 Sept. 2000*, 11(1, pt.1):418–21, 2001.

[43] M.M. Khapaev, A.Yu. Kidiyarova-Shevchenko, P. Magnelind, and M.Yu. Kupriyanov. 3d-mlsi: software package for inductance calculation in multilayer superconducting integrated circuits. *IEEE Transactions on Applied Superconductivity*, 11(1):1090–3, 2001.

[44] O. Nesher and G. Koren. Measurements of delta and v_F from andreev reflections and mcmillan-rowell oscillations in edge junctions of $YBa_2Cu_3O_{6.6}/YBa_2Cu_{2.55}Fe_{0.45}O_y/YBa_2Cu_3O_{6.6}$. *Physical Review B (Condensed Matter)*, 60(13):9287–90, 1999.

[45] J. Mannhart, B. Mayer, and H. Hilgenkamp. Anomalous dependence of the critical current of 45 degrees grain boundaries in $YBa_2Cu_3O_{7-x}$ on an applied magnetic field. *Zeitschrift für Physik B (Condensed Matter)*, 101(2):175–9, 1996.

[46] Y. F. Eltsev, K. Nakao, Y. Yamada, I. Hirabayashi, Y. Ishimaru, K. Tanabe, Y. Enomoto, J. Wen, and N. Koshizuka. Transport properties of bicrystal josephson junctions in Y-Ba-Cu-O films grown by liquid phase epitaxy. *IEEE Transactions on Applied Superconductivity*, 11(1, pt.3):3784–7, 2001. Copyright 2001, IEE.

[47] Y. Ishimaru, J. Wen, T. Utagawa, N. Koshizuka, and Y. Enomoto. Observation of unconventional SQUID-like properties for asymmetrical bicrystal josephson junction. In *Proceedings of 10th International Symposium on Superconductivity, 27-30 Oct. 1997*, volume vol.1 of *Advances in Superconductivity X. Proceedings of the 10th International Symposium*, pages 51–4, Gifu, Japan, 1998. Springer-Verlag Tokyo.

[48] M.A Nielsen and I.L. Chuang. *Quantum Computation and Quantum Information*. Cambridge University Press, 2000.

[49] A.M. Zagoskin. d-wave superconductors and quantum computers. *Physica C*, 368(1-4):305–9, 2002.

[50] A. Blais and A.M. Zagoskin. Operation of universal gates in a solid-state quantum computer based on clean josephson junctions between d-wave superconductors. *Physical Review A (Atomic, Molecular, and Optical Physics)*, 61(4):042308/1–4, 2000.

Appendix A

Energy Conversion Table

The table below lists some experimentally interesting energy values tabulated using four different scales. The conversion between the the scales is done using the following formulas. The voltage-to-frequency conversion is done using the following relations

$$f = \frac{2e}{h}V \tag{A.1}$$

$$T = \frac{2e}{k_B}V \tag{A.2}$$

$$I_c = \frac{2e^2}{h}V \tag{A.3}$$

V	Frequency	Temperature	Critical Current
86 nV	41.7 MHz	1 mK	5.7 pA
1 μV	483 MHz	12 mK	77 pA
2.2 μV	1.02 GHz	25 mK	0.17 nA
10 μV	4.84 GHz	120 mK	0.77 nA
13 μV	5.24 GHz	0.15 mK	1 nA
22 μV	10.8 GHz	260 mK	1.7 nA
86 μV	41.7 GHz	1 K	6.7 nA
100 μV	26.5 GHz	1.2 K	77 nA
0.13 mV	65 GHz	1.6 K	10.4 nA
0.15 mV	70.9 GHz	1.7 K	11 nA
0.21 mV	100 GHz	2.4 K	15nA
0.36mV	175 GHz	4.2 K	28 nA
1mV	484 GHz	12 K	77 nA
6.4 mV	3.2 THz	77 K	0.51 μA
13 mV	6.2 THz	150 K	1 μA
26 mV	12.5 THz	300 K	2.0 μA

Table A.1: Energy conversion table

Appendix B

Numerical Calculations

Numerical calculations are an invaluable tool when working with Josephson devices. Since the equations by their very nature are highly-nonlinear is is almost never possible to find closed analytical solutions. It is however not always straightforward to solve the equations numerically, the governing differential equations are very stiff often nearly singular which means that care has to be taken when choosing the solver.
Here I will give some brief comments on the various calculations used in this work. All computations were done using Matlab.

I_c vs. ϕ for dc-SQUIDs The problem is to maximize eq. 2.30 with respect to ϕ for each ϕ_x. This is done simply by calculating all possible values of eq. 2.30 for a given ϕ_x and then taking the maximum value, by looping over ϕ_x one gets the complete curve

V vs. ϕ for dc-SQUIDs Eq. 2.31 was integrated numerically for each ϕ_x, the only complication is that one needs to use a solver which is unconditionally stable. A trapezoid method was used for simplicity. ¿

I_c vs. ϕ for distributed junctions Basically the algorithm outlined in section 2.5.3 was used directly. It is an optimization problem where one for each value of ϕ_x need to find the value of ϕ which maximizes I_c.

Fitting parameters to experimental I_c vs. ϕ characteristics The problem is to find a set of parameters I_c1^I,I_c1^{II},I_c2^I,I_c2^{II} that minimizes the difference between the theoretical expression eq. 2.30 and the experimental data in a least square sense. The most straightforward way of analyzing the data is to use Fourier analysis, however it turns out that it is difficult to draw any conclusion from such an analysis. Instead the optimization toolbox in Matlab was used. In addition to the four current parameters one also needs a parameter to account for the fact that we do not know the position of the true zero; and also a small parameter that takes into account any excess current in the junctions. In total we have six free parameters. The problem has several possible solutions, depending on the initial conditions so care has to be taken to make sure that a given solution makes sense physically. The best solver for this problem turned out to be 'lsqcurvefit' which is a non-linear curve-fitting algorithm. Using this solver it is also possible to limit the solution-space which is important in order to make sure that the solution is meaningful.

The main problem with the model that was used is that it does not take the Fraunhofer modulation of the junctions into account, doing so would probably give a better result, but at the cost of added complexity.

Appendix C

Appended Papers

Paper I

Feasibility studies of ultra-small Josephson junctions for qubits
A.Ya Tzalenchuk, T. Lindström, S.A. Charlebois, E.A Stepantsov, A.M. Zagoskin, Z. Ivanov and T. Claeson,
IEEE Transactions on Applied Superconductivity, v 13, n 2 (2003)

Feasibility Studies of Ultra-Small Josephson Junctions for Qubits

Alexander Ya. Tzalenchuk, Tobias Lindström, Serge A. Charlebois, Evgueni A. Stepantsov, Alexandre M. Zagoskin, Zdravko Ivanov, and Tord Claeson

***Abstract*—Most proposed realizations of a high temperature superconductor (HTS) qubit (e.g., [1]) require the use of very small Josephson junctions. The properties of bicrystal junctions are especially interesting since they make it possible to implement several types of flux qubits in a relatively simple way.**

We have developed a technique that allows us to produce high quality sub-micrometer junctions in a reproducible way using bicrystal technology. We have successfully fabricated and characterized a large number of YBCO junctions and SQUIDs with bridge width as small as 0.2 micrometer on 0°–3°, 0°–40° and 0°–45° bicrystal STO substrates.

The properties of these junctions have been extensively examined at temperatures down to 20 mK. The effects of external magnetic fields on these structures have been investigated. Figures of merit for the proposed qubits were also extracted from these measurements.

***Index Terms*—D-wave symmetry, high-temperature superconductivity, Josephson effect, quantum computing, sub-micrometer grain boundary Josephson junctions.**

I. Introduction

IT IS WELL known that bicrystal Josephson junctions fabricated on high-angle substrates exhibit a number of unusual features [2], [3]. The fact that most of these properties are direct consequences of the predominant d-wave symmetry of the superconducting wave-function is well established.

Much progress in the field of quantum computing has been achieved over the past few years. A number of groups have successfully demonstrated that it is indeed possible to fabricate the basic building blocks of quantum computers, so-called qubits, using solid-state technology [4]–[6]. Most of these implementations have used superconducting elements as an integral part of their design, yet all of these structures have been fabricated using conventional (i.e., low-T_c) superconductors.

It has been suggested that junctions and SQUIDs fabricated in YBCO might have certain advantages over their conventional counterparts [7]. In phase-qubits, the d-wave symmetry can be used to self-bias the qubit. There are a number of suggested qubit-implementations that uses high-T_c superconductor (HTS) but so far none has been demonstrated experimentally. One of the greatest obstacles has been that the existing technologies for fabrication HTS nanostructures are very limited and the reproducibility is very poor.

We have developed a technique that allows us to produce high quality sub-micrometer junctions in a reproducible way using bicrystal technology. Using this technology we have fabricated and characterized a large number of Josephson junctions and SQUIDs on 0°–30°, 0°–40° and a 0°–45° bicrystal substrates. The bridge width can be as small as 0.2 μm. We have extracted figures of merit for the proposed qubits using our data.

Manuscript received August 6, 2002. The work is supported in parts by D-Wave Systems, Canada, and the Fonds québécois de la recherche sur la nature et les technologies, Canada.

A. Ya. Tzalenchuk is with the National Physics Laboratory. (e-mail: alexander.tzalenchuk@npl.co.uk).

E. A. Stepantsov is with the Institute of Crystallography, Russian Academy of Science, Moscow, Russia.

T. Lindström, S. A. Charlebois, Z. Ivanov, and T. Claeson are with the Department of Microelectronics and Nanoscience, Chalmers University of Technology and Göteborg University, SE-412 96 Göteborg, Sweden. (e-mail: f4azi@fy.chalmers.se)

A. M. Zagoskin is with D-Wave Systems, Canada and the Physics and Astronomy Department, University of British Columbia, Vancouver, Canada.

Digital Object Identifier 10.1109/TASC.2003.814158

II. Theoretical Background

A. D-Wave Symmetry

In the case of an order parameter with d-wave symmetry, the current-phase relation (CPR) of HTS Josephson junctions is not a simple sinusoidal function of the phase but rather the sum of many harmonics. A consequence of the d-wave symmetry is that in 0°–45° grain boundary Josephson junctions (GBJJ) the first harmonic of the CPR is suppressed by symmetry, tunneling from a lobe to a node of the order parameter being forbidden. The supercurrent is then only due to higher harmonics of the CPR, mainly the second.

This simple picture is only valid in the clean ballistic limit. It can however be shown that the 1st harmonic will still be suppressed for a more realistic interface but with a strong temperature dependence [10], [12]. The 2nd harmonic will only dominate below some definite temperature T^*. Any form of scattering will also tend to reestablish the domination of the 1st harmonic. The interplay between the 1st (2π-periodic) and 2nd (π-periodic) harmonics of the CPR of 0°–45° GBJJ has unique effects that could prove to be very useful for qubit implementation.

B. Phase Qubits Utilizing the D-wave Symmetry

There are two classes of superconducting qubits characterized by the ratio of the Josephson energy $(E_J = \Phi_0 I_c/2\pi, \Phi_0 = h/2e)$ to the charging energy $(E_C = e^2/2C)$. The phase qubits are those for which E_J sets the scale of operation $(E_J > E_C)$. An important distinction between the concept described in this paper and phase-qubits based on conventional superconductivity is that in our case the double-well potential, with relevant Josephson energy scale

$E_J^{II} = \Phi_0 I_c^{II}/4\pi$, comes from the *second harmonic* of the current-phase relation.

Phase fluctuations occur at the plasma frequency given by:

$$\hbar\varpi_p = \sqrt{32E_J^{II}E_c} \text{ for } I_c^{II} \gg I_c^I. \quad (1)$$

This can be regarded as an attempt rate to tunnel through the barrier. Two distinct quasiclassical states will exist for $\hbar\varpi_p/2 < E_J^{II}$ or equivalently $\sqrt{32E_c/E_J^{II}} < 1$. The two states will be separated by tunnel splitting:

$$\Delta = \hbar\varpi_p \exp\left(-\sqrt{\frac{E_J^{II}}{E_c}}\right) \text{ for } I_c^{II} \gg I_c^I. \quad (2)$$

The presence of the 2nd harmonics is clearly manifested in SQUID devices. The standard expression for the maximum supercurrent that can flow through a SQUID is

$$I_m = \max_{\gamma_1}\Big\{I_{c1}^I \sin(\gamma_1) + I_{c2}^I \sin(\gamma_1+\phi) - I_{c1}^{II}\sin(2\gamma_1) - I_c^{II}\sin 2(\gamma_1+\phi)\Big\}, \quad (3)$$

with γ_i the phase difference in junction i, $\phi = 2\pi\Phi/\Phi_o$ the magnetic flux contribution and where the indices 1 and 2 represent the junctions and the roman numbers represents the 1st and 2nd harmonic respectively. In this expression we have kept the first harmonic terms to account for remnant contributions from the 1st harmonic (due to imperfections in the interface) in a real device.

C. Size Effects

The design of a real device based on the ideas described above has of course also to consider other effects. Decoherence due to nodal quasiparticles is a major problem in HTS qubits. However, it can be shown that by making the junctions small enough the low-lying excitations will be suppressed by size quantization. In order to achieve a 1 K size induced gap at the Fermi-level one can estimate that the size of the junctions must be

$$d \approx \frac{\hbar v_F}{k_B \cdot 1\text{ K}} \approx 1\ \mu\text{m}. \quad (4)$$

This optimistic estimate is valid only for a ballistic S-N-S junction and assuming a mean free path of the order of hundreds of nanometers (which is certainly possible in a high-quality epitaxial film). A more realistic estimate should probably take into account the smaller mean free path of the grain boundary interface ($l \approx 10$ nm); the spectrum is then gapped by an energy of the order of the Thouless energy which means that the size should be smaller than 100 nm to obtain the 1 K size induced gap. Furthermore, it is well recognized that small junctions have a reduced coupling to the external degrees of freedom.

D. Implementation

Theoretical considerations tell us that in order to successfully fabricate a HTS qubit one has to be able fabricate high-quality sub-micrometer Josephson junctions on high-misorientation angle substrates. Furthermore the 2nd harmonic must dominate so that $\sqrt{32E_c/E_J^{II}} < 1$; this in turn means that one needs to fabricate 0°–45° junctions with a relatively high transparency and low scattering.

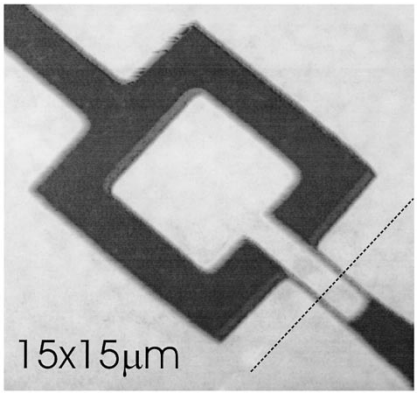

Fig. 1. AFM image of a SQUID with 0.4 μm wide junctions and 15 × 15 μm loop size. The dotted line indicates the grain boundary.

III. Fabrication

The fabrication process has 4 main stages. First, the YBCO thin film is deposited using standard pulsed laser deposition technique and capped *in situ* with a thin (∼20 nm) layer of gold. Further 30 nm of Au thin film is deposited *ex situ*. Contact pads and alignment marks are patterned in 200 nm Au film by using electronresist lift-off stencil defined by e-beam lithography. In the same step, fine rulers (0.5 μm pitch) are produced to enable localization of the grain boundary (GB) with respect to the main alignment marks. The design of the chip is then adjusted to align the junctions according to the actual GB position on the chip. This strategy allows us to achieve a 0.2 μm positioning accuracy with respect to the GB.

The next stage is the patterning of the amorphous carbon mask. We first deposit an amorphous carbon layer (120 nm) by e-beam evaporation. The chip design is patterned by e-beam lithography onto a Cr mask by lift-off. The pattern is then transferred to the a-C mask by oxygen plasma etching through the Cr mask. This step renders a positive a-C mask of the chip on the YBCO which is then ready to be etched by Ar ion milling to form the operational device. The final stage involves stripping the residual a-C mask by oxygen plasma etching and removing the thin Au layer covering the YBCO by a low acceleration Ar ion milling. An AFM image of a SQUID with 0.4 μm wide junctions is presented in Fig. 1 [13].

IV. Experimental Results

A. Sub-Micrometer Josephson Junctions

In a previous study [8] we have fabricated a large number of Josephson junctions of various widths, w, on the sub-micrometer range using the technique outlined above. We were able to achieve a close reproducibility of the junction parameters. While the $j_c\rho_n$ product had the usual $(j_c)^{1/2}$ scaling, the zero-field critical current of the junctions increased approximately as w^2, in the range $w = 0.2$–4 μm (see Fig. 2). The current-voltage characteristics of the junctions were of RCSJ type with observed Shapiro steps. They were hysteretic at low temperatures which allowed us to use the method presented by E. Tarte *et al.* [9] to estimate junction capacitances and hence the Coulomb energy. We have found that the capacitance of sub-micrometer junctions obeys, over an order of magnitude, the $1/R$

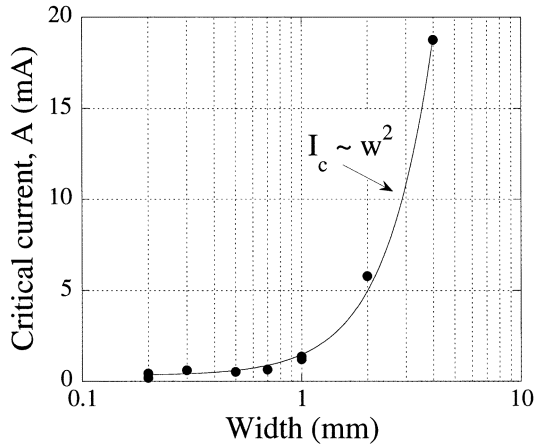

Fig. 2. Critical current as a functions of width for 0°–45° YBCO bicrystal junctions. Measured at 4 K.

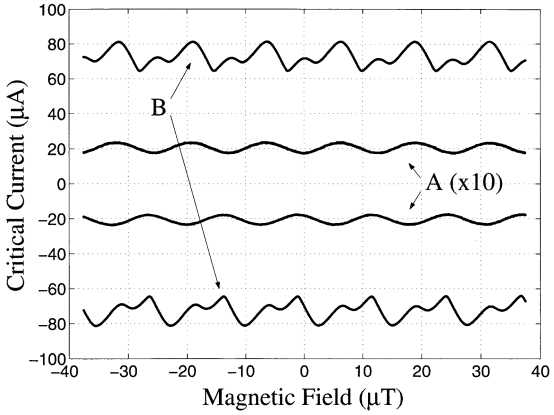

Fig. 3. The critical current as function of applied magnetic field for two SQUIDS with the same loop size (15×15 μm). SQUID A: 0.3/0.2 μm junctions, the values have been multiplied by 10 for clarity. SQUID B: 2/2 μm junctions. All curves measured at 4 K.

scaling determined earlier by Tarte *et al.*. for wide junctions. Following (1) and (2) the Josephson and the Coulomb energies can be estimated. To establish the accuracy of the single-shot measurements of I_c and C we have also studied the distributions of the switching and the retrapping currents at 4 K and 20 mK. The estimated error due to the finite width of the distribution was about 5% for I_c and 30% for C.

B. Second Harmonic in Dc-SQUIDs

In order to estimate α we have fabricated SQUIDs with the junctions 0.2–2 μm wide and the loop size 5–15 μm and measured their critical current as a function of magnetic field. In total 10 SQUIDs of various sizes were measured. All SQUIDs with narrow junctions showed a nearly ideal sinusoidal response to low fields, while all SQUIDs with wide junctions had a pronounced second harmonic, which in some cases was even dominant. An example of this behavior can be seen in Fig. 3. The second harmonic gradually faded away as the field was increased. The main period of the magnetic response for the two types of SQUIDs appeared to be very similar. Previously a substantial second harmonic I_c^{II} at 4 K

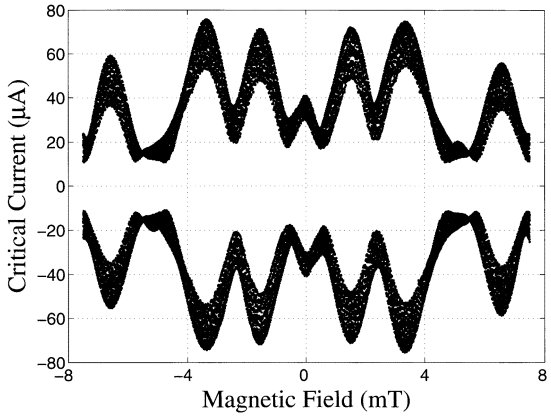

Fig. 4. Critical current as function of applied magnetic field for a SQUID with 2 μm wide junctions and 15×15 μm loop size. Measured at 4 K.

in SQUIDs with 0°–45° bicrystal junctions was reconstructed from the inductive resonance measurements by Il'ichev *et al.* [10].

Critical current of the SQUID junctions measured in a much wider magnetic field range (Fig. 4) demonstrate a pattern perfectly symmetric with respect to the direction of both the field and the bias current, albeit by far not an ideal Fraunhofer pattern. Importantly, the critical current reached its maximum value at fields away from zero. It is widely accepted that this picture arises from a combined effect of a large number of 0 and π facets in the junction [11]. It is worth mentioning that even the widest junctions measured are still magnetically short, as the Josephson penetration length $\lambda_J - \Phi_0/\sqrt{4\pi\mu_0 j_c \lambda_L}$ is about 2 μm and the quasiperiod of the pattern in Fig. 4 is close to $\Phi_0/2\lambda_L w$.

V. Discussion

A stronger than linear dependence of the critical current of the junctions on their width in the sub-micrometer range possibly signals some mechanism of deterioration of the junction properties during processing. Such mechanism can be related to enhanced oxygen out-diffusion along the grain boundary region. Oxygen disorder in the vicinity of a sub-micrometer junction would suppress the d-wave order parameter and establish a small s-wave component. This in turn would decrease the second harmonic of the current-phase relationship as was indeed observed in our experiments at 4 K. In contrast to the disorder scenario, a mere increase of barrier thickness would support the second harmonic of the critical current [12]. It would therefore be instructive to perform post-processing oxygenation of sub-micrometer junctions in an attempt to recover the second harmonic. If this can be achieved, the following parameters of the qubits can be envisaged using 0°–45° bicrystal junctions with width of the order of 100 nm:

- $I_c \approx I_c^I + I_c^{II} \approx 500$ nA, $I_c^I \sim I_c^{II}$
- $E_J^{II}/k_B \approx 3$ K
- $C \approx 10$ fF $\rightarrow E_c/k_b \approx 100$ mK
- $E_J^{II}/E_c \approx 32$
- $\omega_p \approx 390$ ns^{-1}
- $\Delta/k_B \approx 10$ mK or $\Delta/h \approx 0.2$ GHz

VI. Summary

Our measurements of dc-SQUIDs show that the second harmonic of the Josephson current is always present in 2 μm wide 0°–45° bicrystal junctions which is a prerequisite for realization of the discussed qubit. More than 4 chips were fabricated and 80% of the 20 SQUIDs with sub-micrometer junctions on each chip were working. Parameters extracted from the SQUID performance envisage the qubit realization. A number of precautions should be taken however to reach the qubit implementation.

Acknowledgment

The authors would like to thank E. Il'ichev for the discussions and private communications. Samples have been fabricated in the MC2 facilities.

References

[1] A. Blais and A. M. Zagoskin, "Operation of universal gates in a solid-state quantum computer based on clean Josephson junctions between d-wave superconductors," *Physical Review A (Atomic, Molecular, and Optical Physics)*, vol. 61, pp. 042 308/1–4, 2000.

[2] H. Hilgenkamp and J. Mannhart, "Grain boundaries in high-T_c superconductors," *Reviews of Modern Physics*, vol. 74, pp. 297–659, 2002.

[3] T. Löfwander, V. S. Shumeiko, and G. Wendin, "Andreev bound states in high-Tc superconducting junctions," *Superconductor Science & Technology*, vol. 14, pp. R53–77, 2001.

[4] Y. Nakamura, Y. A. Pashkin, and J. S. Tsai, "Coherent control of macroscopic quantum states in a single-Cooper-pair box," *Nature*, vol. 398, pp. 786–8, 1999.

[5] D. Vion, A. Aassime, A. Cottet, P. Joyez, H. Pothier, C. Urbina, D. Esteve, and M. H. Devoret, "Manipulating the quantum state of an electric circuit," *Science*, vol. 296, pp. 886–889, 2002.

[6] C. H. Van Der Wal, A. C. J. Ter Haar, F. K. Wilhelm, R. N. Schouten, C. J. P. M. Harmans, T. P. Orlando, S. Lloyd, and J. E. Mooij, "Quantum superposition of macroscopic persistent-current states," *Science*, vol. 290, pp. 773–7, 2000.

[7] L. B. Ioffe, V. B. Geshkenbein, M. V. Feigel'man, A. L. Fauchere, and G. Blatter, "Environmentally decoupled sds-wave Josephson junctions for quantum computing," *Nature*, vol. 398, pp. 679–81, 1999.

[8] A. Y. Tzalenchuk, T. Lindström, S. Charlebois, S. Stepantsov, and Z. Ivanov, Manuscript.

[9] E. J. Tarte, G. A. Wagner, R. E. Somekh, F. J. Baudenbacher, P. Berghuis, and J. E. Evetts, "The capacitance of bicrystal Jospehson junctions deposited on $SrTiO_3$ substrates," *IEEE Trans. Appl. Superconductivity*, vol. 7, no. 2, 1997.

[10] E. Il'ichev, M. Grajcar, R. Hlubina, I. J. RRJ, H. E. Hoenig, H. G. Meyer, A. Golubov, M. H. S. Amin, A. M. Zagoskin, A. N. Omelyanchouk, and M. Kupriyanov, "Degenerate ground state in a mesoscopic $YBa_2Cu_3O_{7-x}$ grain boundary Josephson junction," *Physical Review Letters*, vol. 86, pp. 5369–72, 2001.

[11] W. K. Neils and D. J. van Harlingen, "Search for complex order parameters in grain boundary junctions," *Physica B*, vol. 284–288, 2000.

[12] Y. S. Barash, "Quasiparticle "Interface states in junctions involving d-wave superconductors," *Physical Review B (Condensed Matter)*, vol. 61, pp. 678–88, 2000.

[13] M. H. S. Amin *et al.*, The Structure is Suggested in a Manuscript.

Paper II

Dynamical Effect of an Unconventional Current-Phase Relation in YBCO dc SQUIDs
T.Lindström, S. A. Charlebois, A. Ya. Tzalenchuk, Z. Ivanov, M. Amin and A.M. Zagoskin
Physical Review Letters 90, 117002 (2003)

Dynamical Effects of an Unconventional Current-Phase Relation in YBCO dc SQUIDs

T. Lindström,[1,*] S. A. Charlebois,[1] A. Ya. Tzalenchuk,[2] Z. Ivanov,[1] M. H. S. Amin,[3] and A. M. Zagoskin[3,4]

[1]*Department of Microelectronics and Nanoscience, Chalmers University of Technology and Göteborg University, SE-412 96 Göteborg, Sweden*

[2]*National Physical Laboratory, Teddington, Middlesex TW11 0LW, United Kingdom*

[3]*D-Wave Systems Inc., 320-1985 Broadway, Vancouver, British Columbia, Canada V6J 4Y3*

[4]*Physics and Astronomy Department, The University of British Columbia, 6224 Agricultural Road, Vancouver, Canada V6T 1Z1*

(Received 20 December 2002; published 17 March 2003)

The predominant *d*-wave pairing symmetry in high-temperature superconductors allows for a variety of current-phase relations in Josephson junctions, which is to a certain degree fabrication controlled. In this Letter, we report on direct experimental observations of the effects of a nonsinusoidal current-phase dependence in YBCO dc SQUIDs, which agree with the theoretical description of the system.

DOI: 10.1103/PhysRevLett.90.117002 PACS numbers: 74.50.+r, 85.25.Dq

It is well established [1] that the wave function of a Cooper pair in most cuprate high-temperature superconductors (HTS) has a *d*-wave symmetry. Its qualitative distinction from, e.g., the anisotropic *s*-wave case is that the order parameter changes sign in certain directions, which can be interpreted as an *intrinsic* difference in the superconducting phase between the lobes equal to π.

The latter leads to a plethora of effects, such as formation of Andreev bound states at surfaces and interfaces in certain crystallographic orientations [2–4]. The current-phase dependence $I_S(\phi)$ in Josephson junctions formed by *dd* junctions, as well as by *sd* junctions comprised of a cuprate and a conventional superconductor, depends both on the spatial orientation of the *d*-wave order parameter with respect to the interface, and on the quality of the latter [5–9]. Time-reversal symmetry can also be spontaneously violated and thus spontaneous currents generated [10–12]. Another effect can be doubling of the Josephson frequency [6,13,14].

In this Letter, we report on experimental observations of strong effects of an unconventional current-phase relation on the dynamics of two *dd* junctions integrated into a superconducting interference device (SQUID) configuration.

Since $I_S(\phi)$ must be a 2π-periodic odd function, it can be expanded in a Fourier series. In most cases, only the first two harmonics give a significant contribution to the current:

$$I_S(\phi) = I_c^{\mathrm{I}} \sin\phi - I_c^{\mathrm{II}} \sin 2\phi. \tag{1}$$

In Josephson systems of conventional superconductors, the second harmonic will usually be negligible [15] but in *dd* junctions the second harmonic may dominate. If $I_c^{\mathrm{II}} > I_c^{\mathrm{I}}/2$, the equilibrium state is no longer $\phi = 0$ but becomes double degenerate at $\phi = \pm \arccos(I_c^{\mathrm{I}}/2I_c^{\mathrm{II}}) \rightarrow \pm\pi/2$. The system can then spontaneously break time-reversal symmetry by choosing either state. Spontaneous currents as well as fluxes can be generated in this state. The potential will have the shape of a double well, and there are reasons to believe that it will be possible to observe quantum coherence in this system. The presence of a second harmonic in the current-phase relation (CPR) of a *dd* junction was confirmed by Il'ichev *et al.* [8].

A nonsinusoidal CPR of the junctions will change the dynamics of a dc SQUID [16]. Regarding the junctions as magnetically small, the supercurrent through the SQUID in the presence of an external flux $\Phi_x \equiv \Phi_0 \cdot (\phi_x/2\pi)$ can be written as

$$I_s(\phi, \phi_x) = I_{c1}^{\mathrm{I}} \sin\phi - I_{c1}^{\mathrm{II}} \sin(2\phi) + I_{c2}^{\mathrm{I}} \sin(\phi + \phi_x) - I_{c2}^{\mathrm{II}} \sin 2(\phi + \phi_x). \tag{2}$$

The critical current through the SQUID is given by the usual expression $I_c(\phi_x) = \max_\phi I_s(\phi, \phi_x)$. The time-averaged voltage over the SQUID in the resistive regime is readily obtained in the resistively shunted junction approximation. By introducing $\delta[\phi, \phi_x] = \phi_2 - \phi_1$ and applying the same method as in [17] with the necessary generalizations, we obtain the following for the average voltage over the SQUID:

$$\overline{V}^{-1} = \frac{G_1 + G_2}{2\pi} \int_{-\pi}^{\pi} d\phi \left[I - (G_1 - G_2) \frac{\hbar}{2e} \frac{d\delta}{dt} - I_1\left(\phi + \frac{\delta}{2}\right) - I_2\left(\phi - \frac{\delta}{2}\right) \right]^{-1}. \tag{3}$$

Here $G_{1,2}$ are the normal conductances of the junctions, and

$$\delta + \phi_x + \frac{\pi L}{\Phi_0} [I_2(\phi - \delta/2) - I_1(\phi + \delta/2)] = 0 \tag{4}$$

gives the difference, δ, in phase drops across each junction. In deriving (3) and (4), we have assumed that the inductance L is equally divided between the SQUID arms. We have also neglected the spontaneous magnetic fluxes in the *dd* junctions, due to their small amplitude [11,18]. Though (4) is only explicitly solvable in the limit

$L \to 0$, it always yields $\delta[-\phi, -\phi_x] = -\delta[\phi, \phi_x]$. This means that the usual inversion symmetry is retained.

The results of numerical calculations based on (2) and (3) are shown in Fig. 1. The cusps in the critical current correspond to the points at which the global maximum in (1) switches from one local maximum to another [16]. Note the quasi-$\Phi_0/2$ periodicity of the current isolines in the $\overline{V} - \phi_x$ picture, reflecting the current-phase dependence (1), and their shift along the Φ_x axis, which depends on the sign of the bias current (as it must to maintain the central symmetry with respect to the origin). The shift does not depend on the magnitude of the current since we neglect the self-inductance. For large biases, the Φ_0 periodicity is restored. Indeed, as the bias grows, one set of minima of the washboard potential, $U = (h/2e)[-I^{\mathrm{I}}\cos\phi + (I^{\mathrm{II}}/2)\cos 2\phi - I\phi]$, disappears first unless the first harmonic I^{I} is *exactly* zero.

We have fabricated and studied a large number of dc SQUIDs. The samples were fabricated from 250 nm thick YBCO films deposited on $SrTiO_3$ bicrystals. The grain-boundary junctions (GBJs) are of the asymmetric [001]-tilt type with the misorientation angle of 45° (0°–45° GBJ). For more information on GBJs see, for example, Ref. [19].

The pattern was defined using *E*-beam lithography and then transferred to a carbon mask employing a multistep process. Finally, the YBCO is etched through the mask using ion milling. This scheme allows us to fabricate high-quality bicrystal junctions as narrow as 0.2 μm, as has been reported elsewhere [20]. In the SQUIDs under investigation, the junctions are nominally 2 μm wide; hence, the fabrication-induced damage of the junctions is small.

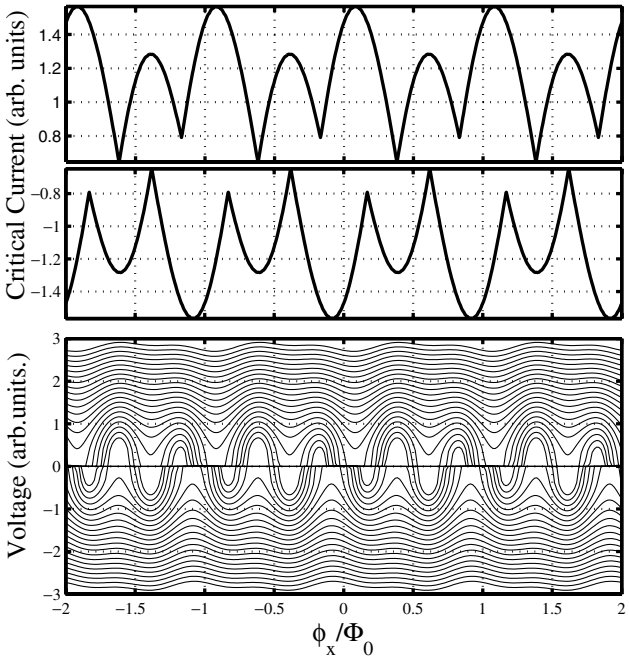

FIG. 1. The results of simulations of the $I_c - \phi_x$ and $\bar{V} - \phi_x$ dependence for a dc SQUID with $I^{\mathrm{I}}_{c1} = 1$, $I^{\mathrm{I}}_{c2} = 0.1$, $I^{\mathrm{II}}_{c1} = 0.2$ and $I^{\mathrm{II}}_{c2} = 0.4$ (arbitrary units). The different curves correspond to bias currents in the range $I = I^{\mathrm{I}}_{c1}$ to $I = 5I^{\mathrm{I}}_{c1}$. We assume $L = 0$ and $G_1 = G_2$.

The measurements were done in an EMC-protected environment using a magnetically shielded LHe cryostat. However, the magnetic shielding is imperfect, as is evident from the fact that the expected zero-field response of our SQUIDs is not exactly at zero. The measuring electronics is carefully filtered and battery powered whenever possible. In order to measure the dependence of the critical current on the applied field, we used a voltage discriminator combined with a sample-and-hold circuit. All measurements reported here were performed at 4.2 K.

The SQUID loops are (15×15) μm^2. The numerically calculated inductance [21] is approximately 25 pH, yielding the factor $\beta = 2\pi L I_c/\Phi_0$ between 0.5–2.

The SQUIDs were largely nonhysteretic with a resistance of about 2 Ω. The measured critical current varies from sample to sample but is in the range of tens of microamperes giving a current density of the order of $J_c = 10^3$ A/cm^2. The estimated Josephson penetration length $\lambda_J = \Phi_0/\sqrt{4\pi\mu_0 j_c \lambda_L}$ is approximately 2 μm in all junctions, which means that the junctions are magnetically short. This is supported by the quasiperiod of the pattern in Fig. 2 being close to the expected value $\phi_0/2\lambda_L w$ [17]. The differential conductance curves do not show any trace of a zero bias anomaly (ZBA), as is expected for 0°–45° GBJs. ZBAs have been observed by other groups in GBJs with other orientations [2].

The critical current is plotted as a function of applied magnetic field for two SQUIDs in Fig. 3. The result is in qualitative agreement with theory if we assume that the SQUID junctions have different ratios of the first and second harmonics of the critical current. This assumption

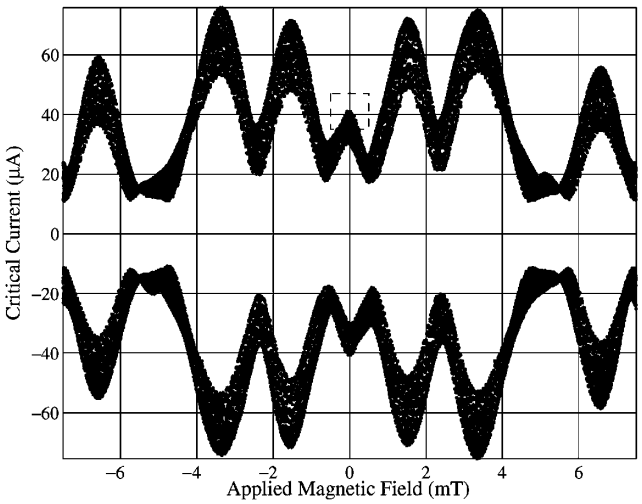

FIG. 2. Critical current as a function of magnetic field at 4.2 K. The dashed box indicates the area plotted in Fig. 3(a).

is supported by the fairly small modulation depth [it is easy to see from Eq. (2) that I_c would go exactly to zero in a SQUID with junctions of identical I_{c2}/I_{c1}].

We can fit the data to Eq. (2), if we compensate for the residual background magnetic field and assume that we have a small excess current (of the order of a few μA) in the junctions. The fitting parameters again confirm that there is a large asymmetry between the arms of the SQUIDs. Note that the model does not consider the flux penetration into the junctions,

The result for fields of the order of mT is presented in Fig. 2, which shows the I_c modulation of the SQUID enveloped by an anomalous Fraunhofer pattern quite similar to what has been reported by other groups [22,23] for 0°–45° GBJs. Note the inversion symmetry of the pattern with respect to the origin. That the global maximum is not in the center can be explained in several ways; it has been shown, for example, that this could be due to the presence of so-called π loops in the junction interface [24].

Figure 4 shows the V-B dependence of one of the SQUIDs. The pattern is again field inversion symmetric. The overall structure is the same as in the model dependence of Fig. 1, but there is also an additional shift due to self-field effects, which depends on the magnitude of the bias current and corresponds (at maximum) to a flux $\sim 0.1\Phi_0$. In a beautiful experiment, a similar dependence was recently observed by Baselmans *et al.* in a Nb-Ag-Nb SNS junction where current injectors were used to change the occupation of current-carrying states in the normal region [25]. A deviation from the model occurs at $\overline{V} = 100\ \mu$V where the minima and maxima switch. This is probably due to an LC resonance in the SQUID. Taking $L = 25\ p$H, this would require $C = 0.8\ pF$, which agrees with our measurements on single junctions

Remarkably, the observed offset of the V-B characteristics with respect to the *direction* of the bias current appears to be a much more robust manifestation of the presence of a second harmonic of the Josephson current than the shape of the $I_c - B$ curves itself. We observed the shift even in SQUIDs with the smallest junctions down to 0.5 μm wide, where the deviations from the usual sinusoidal CPR were not obvious from the $I_c - B$ dependence.

Generally, the nature of the transport through a GBJ will depend on its transmissivity D. Il'ichev *et al.* [8] have reported values of D as high as 0.3 in symmetric (22.5°–22.5°) *dd* junctions as opposed to the usual estimate for a GBJ, $D \sim 10^{-5}$–10^{-2}. Since usually $I_c^{\mathrm{II}}/I_c^{\mathrm{I}} \propto D$, a high-transmissivity GBJ is required in order

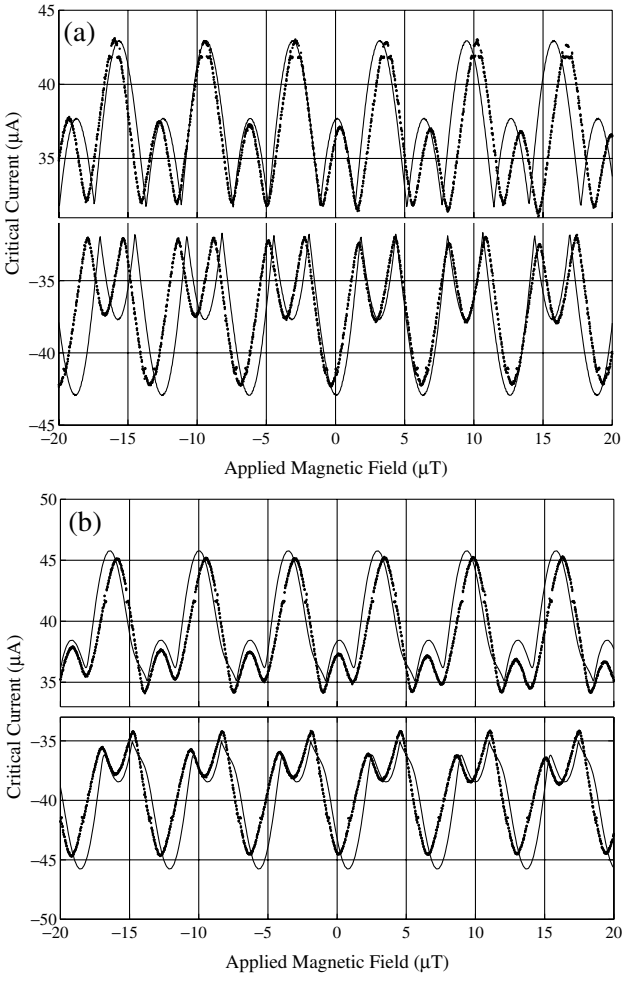

FIG. 3. Critical current as a function of applied magnetic field for two different SQUIDs that are nominally identical. The solid line represents the fitted expression. The fitting parameters are as follows: (a) $I_{c1}^{\mathrm{I}} = 9\ \mu$A, $I_{c2}^{\mathrm{I}} = 0.3\ \mu$A, $I_{c1}^{\mathrm{II}} = 3.7\ \mu$A, and $I_{c2}^{\mathrm{II}} = 22.7\ \mu$A; (b) $I_{c1}^{\mathrm{I}} = 7.8\ \mu$A, $I_{c2}^{\mathrm{I}} = 3.0\ \mu$A, $I_{c1}^{\mathrm{II}} = 5.3\ \mu$A, and $I_{c2}^{\mathrm{II}} = 4.3\ \mu$A. In both cases, the fit has been adjusted with respect to the residual background field and the excess current of the junctions.

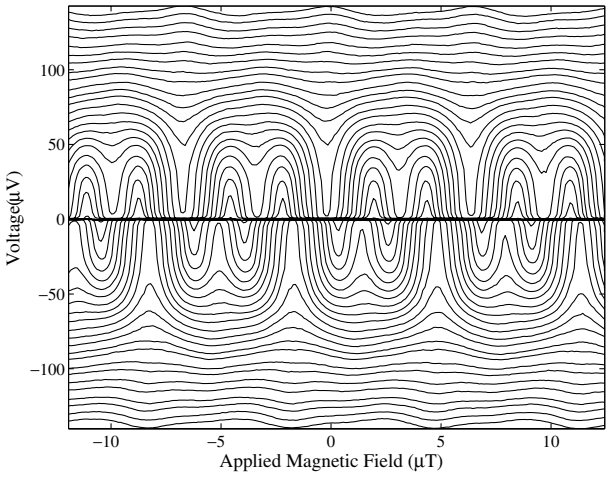

FIG. 4. Voltage modulation as a function of applied magnetic field for the SQUID whose $I_c - B$ is shown in Fig. 3(a). The pattern is again inversion symmetric. Note the sign change at 100 μV, which we believe is due to a LC resonance in the SQUID loop.

to observe effects of the second harmonic. An estimate of the *average* transmissivity of our junctions would be $\rho_{ab} l/R_N A \sim 10^{-2}$ [26] assuming l, the mean-free path, to be equal to 10 nm and a resistivity in the a-b plane ρ_{ab} equal to $10^{-4}\ \Omega\,\mathrm{cm}$. This is still too low to explain the strong second harmonic we observe. However, it is known from, e.g., TEM studies [19], that the grain-boundary is far from uniform; the properties can significantly vary depending on the local properties of the interface, effects such as oxygen diffusion out of the GB, etc., which are difficult to control. It is therefore reasonable to assume that there are many parallel transport channels through the GB [27,28]. Channels with high-transmissivity dominate the transport and might have $D \sim 0.1$ even though the *average* transmissivity is much lower. This is also consistent with the fact that most of our SQUIDs seem to be highly asymmetrical which is to be expected if the distribution of channels is random. The ratios of I_c^{I} and I_c^{II} can vary as much as 10 times between two junctions in the same SQUID, even though the fluctuations of the *total* I_c from sample to sample are much smaller. It is also clear from general considerations that a high value of I_c^{II} *excludes* a high value of I_c^{I}, since the second harmonic usually dominates if the odd harmonics of the supercurrent are canceled by symmetry [29].

Recent studies of 0°–45° GBJs have demonstrated that the SQUID dynamics can be altered by the d-wave order parameter in YBCO [30]. It is, however, important to point out that our results *do not* directly relate to, e.g., tetracrystal π-SQUID experiments; the latter crucially depend on having one π junction with negative critical current, but still only the first harmonic present in $I_c(\phi)$. Our SQUIDs have a conventional geometry, but unconventional current-phase relations.

One explanation for the pronounced effects of the second harmonic could be that relatively large sections of the interface are highly transparent and have a low degree of disorder. This in turn could be related to our fabrication scheme which seems to preserve the integrity of the barrier. This makes feasible their applicability in the quantum regime and supports our expectations that quantum coherence can be observed in this kind of structures.

In summary, we have observed a very pronounced second harmonic in the current-phase relation of a "conventional" YBCO dc SQUID with 0°–45° grain-boundary junctions. It has strongly influenced the SQUID dynamics. All details of the SQUID behavior were explained within a simple model of a *dd* junction with relatively high transparency. We believe that these effects are important for better understanding of HTS Josephson junction and SQUIDs.

Discussions with Evgeni Il'ichev, Alexander Golubov, Tord Claeson, and John Gallop are gratefully acknowledged. The work is in part supported by The Board for Strategic Research (SSF) via the "OXIDE" program, the Science Research Council, and the "Fonds québécois de la recherche sur la nature et les technologies." The processing work is done at the MC2 process laboratory at Chalmers University of Technology.

*Electronic address: tobiasl@fy.chalmers.se

[1] C. Tsuei and J. Kirtley, Rev. Mod. Phys. **72**, 969 (2000).
[2] L. Alff *et al.*, Phys. Rev. B **58**, 11 197 (1998).
[3] T. Löfwander, V. Shumeiko, and G. Wendin, Supercond. Sci. Technol. **14**, R53 (2001).
[4] C.-R. Hu, Phys. Rev. Lett. **72**, 1526 (1994).
[5] S. Yip, Phys. Rev. B **52**, 3087 (1994).
[6] A. Zagoskin, J. Phys. Condens. Matter **9**, L419 (1997).
[7] E. Il'chev *et al.*, Phys. Rev. B **60**, 3096 (1999).
[8] E. Il'ichev *et al.*, Phys. Rev. Lett. **86**, 5369 (2001).
[9] P. Komissinski *et al.*, Europhys. Lett. **57**, 585 (2002).
[10] A. Huck, A. van Otterlo, and M. Sigrist, Phys. Rev. B **56** 14163 (1997).
[11] M. H. S. Amin, A. N. Omelyanchouk, and A. M. Zagoskin, Phys. Rev. B **63**, 212502 (2001).
[12] S. Östlund, Phys. Rev. B **58**, R14 757 (1998).
[13] T. Löfwander, G. Johansson, M. Hurd, and G. Wendin, Phys. Rev. B **57**, R3225 (1998).
[14] H. Arie *et al.*, Phys. Rev. B **62**, 11 864 (2000).
[15] M. Keene, C. Gough, and A. Rae, J. Phys. Condens. Matter **3**, 6079 (1991).
[16] M. H. S. Amin, M. Coury, and R. Rose, IEEE Trans. Appl. Supercond. **12**, 1877 (2002).
[17] A. Barone and G. Paterno, *Physics and Applications of the Josephson Effect* (Wiley, New York, 1982).
[18] M. H. S. Amin, S. N. Rashkeev, M. Coury, A. N. Omelyanchouk, and A. M. Zagoskin, Phys. Rev. B **66**, 174515 (2002).
[19] H. Hilgenkamp and J. Mannhart, Rev. Mod. Phys. **74**, 297 (2002).
[20] A. Tzalenchuk *et al.*, Appl. Phys. Lett. (to be published).
[21] M. Khapaev, A. Kidiyarova-Shevchenko, P. Magnelind, and M. Kupriyanov, IEEE Trans. Appl. Supercond. **11**, 1090 (2001).
[22] J. Mannhart, B. Mayer, and H. Hilgenkamp, Z. Phys. B **101**, 175 (1996).
[23] W. Neils and D. van Harlingen, Physica (Amsterdam) **284B–288B**, 587 (2000).
[24] H. Smilde *et al.*, Phys. Rev. Lett. **88**, 057004 (2002).
[25] J. Baselmans, T. Heikkilä, B. van Wees, and T. Klapwijk, Phys. Rev. Lett. **89**, 207002 (2002); the pronounced second harmonic in this experiment appears due to nonequilibrium effects, see, e.g., J. C. Clarke, in *Nonequilibrium Superconductivity, Phonons and Kapitza Boundaries*, edited by K. E. Gray, NATO ASI Series (Plenum, New York, 1981), p. 353.
[26] G. Blonder, M. Tinkham, and T. Klapwijk, Phys. Rev. B **25**, 4515 (1982).
[27] Y. Naveh, D. Averin, and K. Likharev, Phys. Rev. Lett. **79**, 3482 (1997).
[28] E. Sarnelli, G. Testa, and E. Esposito, J. Supercond. **7**, 387 (1994).
[29] Y. Barash, Phys. Rev. B **61**, 678 (2000).
[30] B. Chesca *et al.*, Phys. Rev. Lett. **88**, 177003 (2002).

Paper III

Mesoscopic Josephson Junctions of high-Tc Superconductors
A. Ya. Tzalenchuk, T. Lindström, S.A. Charlebois, E.A. Stepantsov, Z. Ivanov and A.M. Zagoskin,
Physical Review B 68 100501(R) (2003)

PHYSICAL REVIEW B **68**, 100501(R) (2003)

Mesoscopic josephson junctions of high-T_c superconductors

A. Ya. Tzalenchuk*
National Physical Laboratory, Queens Road, Teddington, Middlesex TW11 0LW, United Kingdom

T. Lindström, S. A. Charlebois, E. A. Stepantsov,† and Z. Ivanov
Department of Microelectronics and Nanoscience, Chalmers University of Technology and Göteborg University, SE-412 96 Göteborg, Sweden

A. M. Zagoskin‡
D-Wave Systems Inc., 320-1985 Broadway, Vancouver, British Columbia, Canada V6J 4Y3

(Received 14 April 2003; published 5 September 2003)

In this paper we examine the state-of-the-art patterning techniques for fabrication of ultrasmall bicrystal Josephson junctions in $YBa_2Cu_3O_x$. We determine the dependence of junction parameters—critical current, characteristic voltage I_cR_n, and capacitance—on its size. Using the values of the Josephson and the Coulomb energies extracted from experiment, we analyze the dynamics of the junction in zero-bias quantum regime. Finally, we discuss the relevance of parameters, obtained from transport measurements, for the decoherence time in the system.

DOI: 10.1103/PhysRevB.68.100501 PACS number(s): 74.50.+r

I. INTRODUCTION

It is well known that quantum effects gain importance in mesoscopic Josephson junctions.[1] This academic fact was pressed home by recent spectacular demonstrations of macroscopic quantum coherence in Josephson devices (qubit prototypes).

Despite early proposals for qubits based on high-T_c superconductors (HTS's),[2,3] these devices remain in the shadow to a large extent because of the lack of a reliable technology to fabricate structures on the submicrometer scale. Earlier attempts mostly concentrated on making small microbridges without weak links and were largely successful.[4–6] Superconducting microbridges down to 50 nm width were fabricated and characterized.[7] These works demonstrated that in spite of the fragility of the stoichiometry of HTS materials, a high quality epitaxial film can withstand patterning to submicrometer size. When it comes to junctions however, the faster rate of oxygen out-diffusion along grain boundaries and interfaces leads to degradation of superconducting properties as the junction size decreases. Nevertheless, recently, preparation of submicrometer step-edge[8] and ramp[9] Josephson junctions was reported. To the best of our knowledge, the first detailed study of bicrystal Josephson junction of a submicrometer size was presented by Elsner *et al.*[10] Lately, bicrystal grain-boundary Josephson junctions in very thin films were demonstrated.[11]

Dynamics of a small Josephson junction is determined by the interplay of charge and phase degrees of freedom. In the limit, where the phase is a good semiclassical variable, the system can be represented by a fictitious quantum particle with the kinetic energy determined by the capacitance of the junction (Coulomb energy E_C), moving in the potential landscape determined by the phase-dependent critical current (Josephson energy $E_J \gg E_C$). The current-phase relation (CPR) in HTS junctions reflects the complicated symmetry of superconducting wave function and appears to be strongly nonsinusoidal.[12,13] So far the analysis of the influence of this anomalous CPR on the dynamics of mesoscopic junctions was restricted by the lack of experimental data. In this paper we present our version of submicrometer technology for HTS films and investigate ultrasmall bicrystal Josephson junctions in $YBa_2Cu_3O_x$ (YBCO) having in mind their proposed qubit applications.

II. EXPERIMENT

We have fabricated a large number of submicrometer junctions and superconducting quantum interference device on $SrTiO_3$ bicrystals with misorientation angles of 0/32°, 0/40°, and 0/45°. Nominally 250-nm-thick YBCO films were grown by laser ablation using standard parameters. Note that our films are ten times thicker than those studied by Herbstritt *et al.*[11] We believe that relatively thick and short microbridges contain enough oxygen to self-heal the oxygen loss in the grain boundary. In order to protect the film surface and improve adhesion of the post-deposited layers, a 10-nm-thick layer of gold was pulsed laser deposited *in situ* on top of YBCO at room temperature, followed by *ex situ* evaporation of additional 40 nm of gold. Two steps of *e*-beam lithography on polymethyl methacrylate/copolymer double-layer resist were sufficient for fabrication. Resist baking was performed at 135 °C—close to the lower limit for this resist type. Reduced resist baking temperature and the minimum number of processing steps at elevated temperatures minimize oxygen loss. In the first *e*-beam lithography we fabricated gold pads for electrical connections and defined gold alignment marks and rulers for the subsequent processing stages, both 250 nm thick. Since the grain boundary does not give contrast under the electron beam, this pattern was aligned only with respect to the chip corners. Readings were taken from the intersection of the grain boundary with the rulers in an optical microscope, where the grain boundaries are visible due to imperfections and sometimes

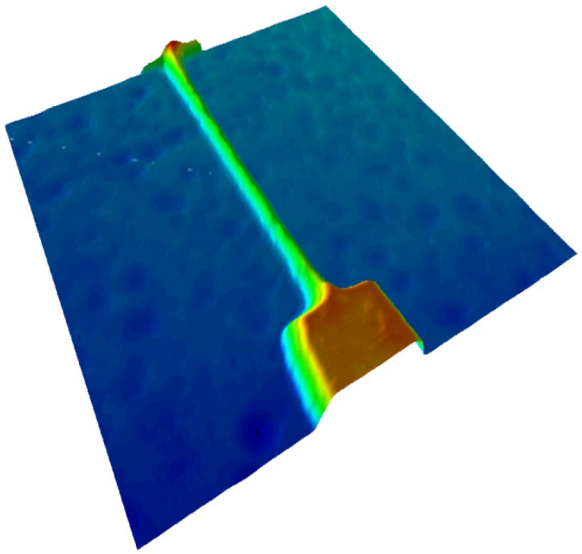

FIG. 1. (Color online) $8\times8\times0.468\ \mu m^3$ atomic force microscope image of a 100-nm-wide bicrystal Josephson junction—the smallest we can make at this time.

due to induced birefringence. The shift and the rotation of the grain boundary with respect to the rulers was then taken into account in the next *e*-beam lithography, which defined the carbon mask for fabrication of the bridges across the bicrystal grain boundary. Alignment could be made with accuracy close to 0.2 μm across the whole substrate. NiCr was used as a masking layer for oxygen plasma etching of carbon. The YBCO was Ar-ion beam etched through the carbon mask during 2 h at 400 eV and 0.1 mA/cm^2. While etching, the substrate was thermally anchored to a 9 °C cold plate to avoid heating and degeneration of the YBCO. Finally, the gold protection layer covering the YBCO was removed by 15-min Ar ion-beam etching at 150 eV and 0.1 mA/cm^2. The result of the completed fabrication process is shown in Fig. 1. It is worth mentioning that even the narrowest of thus prepared junctions are very stable, surviving to-date up to two years without noticeable change in parameters.

III. RESULTS

The dynamical parameters of a mesoscopic Josephson junction can be expressed as a combination of E_J and E_C or explicitly as a function of the critical current I_c and the junction capacitance C. We have measured these parameters at 4.2 K on a large number of Josephson junctions of different dimensions ranging from 0.2 to 4 μm.

In general the critical current of submicrometer junctions did not scale strictly proportionally to the width even though reproducibility in I_c and the normal resistance R_n close to 10% junction to junction on one chip was observed. At the same time the usual scaling of $I_cR_n=j_c\rho_n\propto\sqrt{j_c}$ was confirmed on a large number of submicrometer junctions on different bicrystals (see inset in Fig. 2). Two distinct regions with different slopes can be seen in Fig. 2 with the crossover almost exactly at 1 μm. The crossover might be related to the processing induced damage of the junctions. Interest-

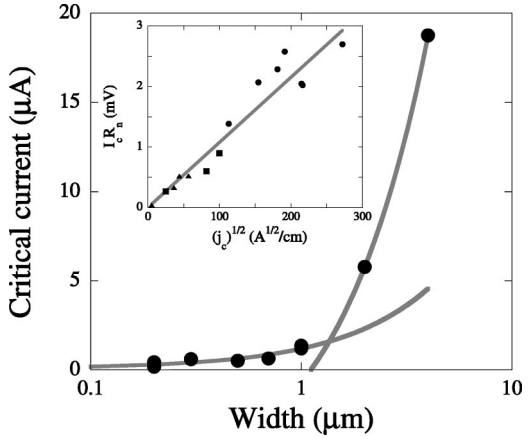

FIG. 2. Critical current as a function of junction width for a 45° grain-boundary junction. The lines are the best linear fits to the data below and above 1 μm; Inset: Scaling of the I_cR_n product with the $\sqrt{j_c}$ measured on two 0/32° and two 0/40° samples.

ingly, however, the large-junction line projects to a finite size of the junction for zero critical current, while the dependence for submicrometer junctions points almost exactly to zero. We therefore speculate that the latter line represents intrinsic properties of the junction barrier, while some other mechanism comes into play on the micrometer scale. For example, this mechanism can be related to high-j_c "shorts" in the barrier.

Most junctions studied in this work were hysteretic by an amount $(I_c-I_r)/I_c\leqslant30\%$ (I_c and I_r are the critical and retrapping currents correspondingly). Applicability of the resistively capacitively shurted junction (RCSJ) model, or equivalently the underlying tilted-washboard potential model, to the dynamics of submicrometer junctions was verified by studying the histograms of the stochastic switching processes between the superconducting and the resistive states of the hysteretic junctions at finite temperatures. The switching currents were determined on successive current sweeps ($\dot{I}\simeq0.1$–10 mA/s) either directly, using a voltage discriminator combined with a sample-and-hold circuit, or from time-of-flight measurements. As can be seen in Fig. 3 (inset) the distributions can be fairly well approximated by the RCSJ expressions. Within this model the junction capacitance can be estimated from the amount of hysteresis following the approximate expression[14] for the Stewart-McCumber parameter

$$\beta_c\equiv(\omega_pR_nC)^2\approx\frac{2-(\pi-2)(I_r/I_c)}{(I_r/I_c)^2},$$

where ω_p is the Josephson plasma frequency. The results for the 40° bicrystal junctions on two different chips are summarized in Fig. 3. As has been previously observed for much wider junctions, the capacitance inversely scales with the junction resistance, yielding $R_nC\simeq1$ ps. In the following section we will provide arguments why this very small time constant does not necessarily spell doom for qubit applications of HTS devices. The values of the junction capacitance are in close agreement with those reported in Ref. 15 for the

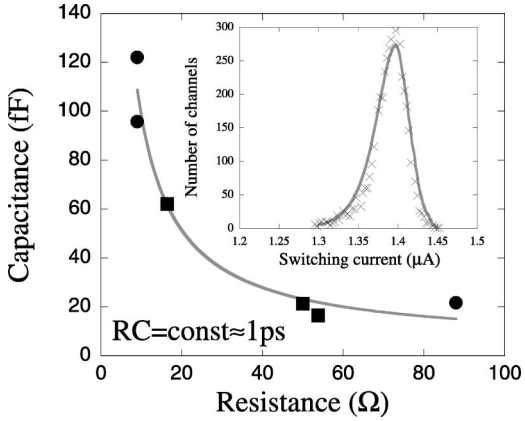

FIG. 3. The junction capacitance as a function of its resistance measured on two 0/40° chips (circles and squares). The best-fit line corresponds to $R_nC \simeq 1$ ps. *Inset*: An experimental switching current distribution histogram and the best fit to the RCSJ model.

junctions of similar resistance. Using the switching histograms, we can estimate the accuracy of parameters determined from single-shot measurements. As can be seen from the figure, the I_c distribution is rather narrow, full width at half maximum equal to (5–7)% of the mean value, which gives the relative error in C determined from the approximation[14] of the order of (30–40)%.

IV. DISCUSSION

Let us first calculate the parameters of submicrometer Josephson junctions, which follow from our experiments. The relation between the Josephson current, energy, and phase difference γ, $I_J(\gamma)=(2e/\hbar)\partial E_J/\partial\gamma$, follows from gauge invariance (and Cooper pair charge being $2e$) and, of course, does not depend on the exact form of $E_J(\gamma)$. Therefore, the nth harmonic of the Josephson energy is related to the nth harmonic of the critical current through $E_{nJ}(\gamma) = \pm\hbar I_n \cos(n\gamma)/2en$. Keeping only the first two harmonics of the current-phase relation, and introducing $\alpha = I_2/I_1$, we reduce the problem to solving the one-dimensional Schrödinger equation for a particle of mass $(\hbar/2e)^2 C$ in thej potential

$$E_J(\gamma) = -E_{1J}\cos(\gamma) + E_{2J}\cos(2\gamma) = -E_{1J}\left[\cos(\gamma) - \frac{\alpha}{2}\cos(2\gamma)\right]. \quad (1)$$

The Hamiltonian of the system is $H = -4E_C\partial_\gamma^2 + E_J(\gamma)$. The ground-state energy of an isolated quantum well is $\hbar\omega_p/2$, where $\hbar\omega_{p1} = 2\sqrt{2E_CE_{1J}}$ for $\alpha \ll 1$, and $\hbar\omega_{p2} = 4\sqrt{2E_CE_{2J}}$ for $\alpha \gg 1$. In order to estimate the tunneling between the minima of E_J, made possible by the "kinetic" Coulomb term, we find the splitting of the energy levels of the two adjacent quantum wells[16] by integrating the momentum $p(E,\gamma)$ between the classical turning points $\pm\gamma_0$ [we neglect the effects of band formation due to periodicity of $E_J(\gamma)$]:

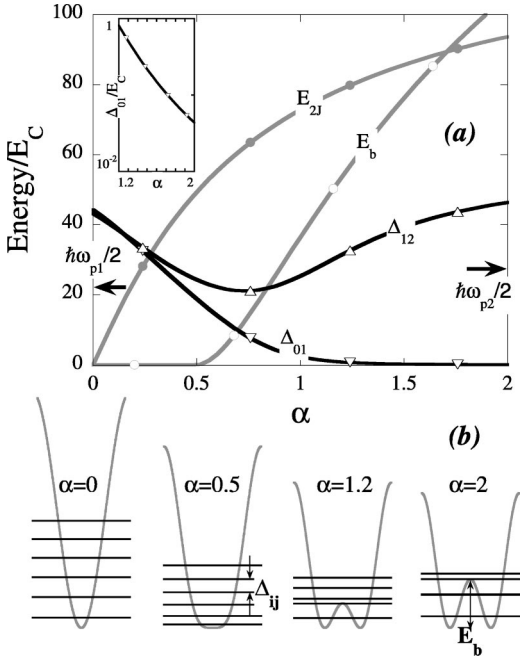

FIG. 4. (a) Level splitting, energy of the second harmonic of the Josephson current, and the barrier height of the double-well potential depending on $\alpha = I_2/I_1$. Arrows indicate the quasiclassical ground-state energies $\hbar\omega_{p1,2}/2$, which are only valid in their respective limits of α. *Inset*: Δ_{01} in more details. (b) Energy level diagrams for several values of α.

$$\Delta \equiv \Delta_{01} = \frac{\hbar\omega_p}{\pi}\exp\left[-\frac{1}{\hbar}\int_{-\gamma_0}^{\gamma_0}\left|p(\hbar\omega_p/2,\gamma)\right|d\gamma\right] = \frac{\hbar\omega_p}{\pi}\exp\left[-\frac{1}{2}\int_{-\gamma_0}^{\gamma_0}d\gamma\sqrt{\frac{E_J(\gamma)-\hbar\omega_p/2}{E_C}}\right]. \quad (2)$$

For example, if the second harmonic dominates, we obtain

$$\Delta = \frac{\hbar\omega_p}{\pi}\exp\left(-\left[\frac{2E_{2J}}{E_C}\right]^{1/2}F\left(\sqrt{2E_C/E_{2J}}\right)\right), \quad (3)$$

where $F(z) = \sqrt{1-z}E[\arccos\sqrt{z}|(1-z)^{-1}]$, and $E(a|b)$ is the elliptic integral of second kind.

In reality $\alpha \approx 1$, and we have to calculate the eigenstates numerically. For a given α, the amplitude of the first harmonic of the Josephson current can be obtained from the measured critical current $I_c \approx 1\ \mu$A, using $I_c = I_1 \max_\gamma\{\sin(\gamma) - \alpha\sin(2\gamma)\}$. The capacitance of the junction was taken to be 10^{-14} F (Fig. 3), corresponding to $E_C/k_B \approx 93$ mK. The results of numerical calculations of different energies as a function of α for this choice of I_c and C are presented in Fig. 4. Above $\alpha = 0.5$ the potential becomes bistable, and as the barrier height E_b increases, so does the spacing between the ground state (split by tunneling) and the higher excited levels. This makes the junction a quasi-two-level system, since the transitions to the higher levels are suppressed. Indeed, for α in the range 1.2–1.7 the splitting between the first and second eigenvalues (100 mK) is one to two orders of magnitude less than the energy difference with the next eigenvalue (>3 K). They can therefore be consid-

ered well decoupled for sub-Kelvin operating temperatures. As an example, for $\alpha=1.2$, $I_c=1$ μA and $C=10^{-14}$ F we obtain the following: $E_C=e^2/2C$ corresponds to 2 GHz or 100 mK; $I_1=0.5$ μA; $I_2=0.6$ μA; $E_{1J}/E_C=131$; $E_{2J}/E_C=79$; $\hbar\omega_p=15$–$25E_C$ (30–50 GHz); $\Delta_{01}/E_C=0.8$ (1.6 GHz or 80 mK), and $\Delta_{12}/E_C=32$ (64 GHz or 3.2 K).

The question of decoherence rate in HTS junctions is still not resolved, though the possibility to observe coherent quantum behavior in these systems hinges on the answer to it. As we noted above, the transport measurements provide the R_nC constant of the order of 1 ps, seemingly closing the door on any possibility to use the HTS materials as quantum bits. Nevertheless such a conclusion could be too hasty. Recently, the decoherence in d/d junctions was considered theoretically.[17] These results question the relevance of R_nC as a measure of damping at zero bias. Indeed, R_n is obtained in the resistive regime, when the phase runs along the washboard potential, and dissipative quasiparticle current is always present. On the contrary, in the ''qubit'' regime the external bias is absent, and the phase is localized. The quasiparticle current only arises due to tunneling between the minima of the potential, which produces ac Josephson voltage: $I(V=\hbar\omega/e=\Delta_{01}/e)$. The main contributions to this low-bias quasiparticle current will be given by midgap Andreev bound states (MGS's) and nodal quasiparticles. The significance of each of these factors depends on the mismatch angle, type of the grain boundary (symmetric or asymmetric), roughness of the interface, and its transparency. As shown by Fominov and Golubov, the most dangerous contribution is due to MGS-to-MGS scattering leading to a zero-bias conductance peak. However, MGS's can be split by several mechanisms, which shifts this peak to higher biases and therefore suppresses this decay channel (for a discussion of phenomena related to Andreev bound states, see the detailed review[18] and references therein). The nodal quasiparticles contribute much less close to zero bias, since this term scales as ω^2. Experimental I-V characteristics of 0/45° grain-boundary junctions (where MGS's are formed only on one side of the interface and therefore only MGS-to-node contribution is significant) show significantly suppressed admittance close to zero bias compared to R_n.

To summarize this discussion, the value of quasiparticle resistance R_n, determined from transport measurements and used above as the natural scaling parameter for the capacitance, is likely irrelevant to decoherence in d/d junctions. On the contrary, the energies E_J and E_C, derived from the same measurements, are correct.

ACKNOWLEDGMENTS

We are indebted to A. Golubov and Ya. Fominov for communicating their results prior to publication and many helpful comments. Discussions with M. H. S. Amin, T. Claeson, J. C. Gallop, A. Maassen van den Brink, and A. Yu. Smirnov are gratefully acknowledged.

*Email address: alexander.tzalenchuk@npl.co.uk

†On leave from Institute of Crystallography, Russian Academy of Sciences, 59 Leninski pr., 117 333 Moscow, Russia.

‡Also at Physics and Astronomy Dept., The University of British Columbia, 6224 Agricultural Rd., Vancouver, Canada V6T 1Z1.

[1] M. Tinkham, *Introduction to Superconductivity*, 2nd ed. (McGraw-Hill, New York, 1996), Chap. 7.

[2] L. Ioffe, V. Geshkenbein, M. Feigel'man, A. Fauchre, and G. Blatter, Nature (London) **398**, 679 (1999).

[3] A. Blais and A. Zagoskin, Phys. Rev. A **61**, 042308 (2000).

[4] R. Barth, B. Spangenberg, C. Jaekel, H. Roskos, H. Kurz, and B. Holzapfel, Appl. Phys. Lett. **63**, 1149 (1993).

[5] J. Schneider, H. Kohlstedt, and R. Wordenweber, Appl. Phys. Lett. **63**, 2426 (1993).

[6] H. Assink, A. Harg, C. Schep, N. Chen, D. Marel, P. Hadley, E. Drift, and J. Mooij, IEEE Trans. Appl. Supercond. **3**, 2983 (1992).

[7] P. Larsson, B. Nilsson, and Z. Ivanov, J. Vac. Sci. Technol. B **18**, 25 (2000).

[8] P. Larsson, A. Tzalenchuk, and Z. Ivanov, J. Appl. Phys. **90**, 3450 (2001).

[9] P. Komissinski, B. Hogberg, A. Tzalenchuk, and Z. Ivanov, Appl. Phys. Lett. **80**, 1022 (2002).

[10] H. Elsner, R. Ijsselsteijn, W. Morgenroth, H. Roth, and H.-G. Meyer, Microelectron. Eng. **41-42**, 407 (1998).

[11] F. Herbstritt, T. Kemen, L. Alff, A. Marx, and R. Gross, Appl. Phys. Lett. **78**, 955 (2001).

[12] E. Il'ichev *et al.*, Phys. Rev. Lett. **86**, 5369 (2001).

[13] T. Lindström, S. Charlebois, A. Tzalenchuk, Z. Ivanov, M. Amin, and A. Zagoskin, Phys. Rev. Lett. **90**, 117002 (2003).

[14] H. Zappe, J. Appl. Phys. **44**, 1371 (1973).

[15] P. McBrien, R. Hadfield, W. Booij, A. Moya, M. Blamire, E. Tarte, J. Clark, and C. Pegrum, IEEE Trans. Appl. Supercond. **9**, 3468 (1999).

[16] L. Landau and E. Lifshitz, *Quantum Mechanics: Non-relativistic Theory*, 3rd ed. (Pergamon Press, Oxford, 1977), Vol. 3, Chap. 7, sec. 50.

[17] A. Golubov and Y. Fominov (unpublished); M.H.S. Amin (private communication); A.N. Omelyanchouk, Yu. Kolesnichenko, and A.M. Zagoskin (private communication).

[18] T. Löfwander, V. Shumeiko, and G. Wendin, Supercond. Sci. Technol. **14**, R53 (2001).